

Department of Physics and Astronomy
University of Heidelberg

Bachelor Thesis in Physics
submitted by

Felix Benjamin Schäfer

born in Mannheim (Germany)

2012

Polarization Effects on Detector Acceptance in

$$D^{*+}(2010) \rightarrow D^0(K^-\pi^+) + \pi^+$$

This Bachelor Thesis has been carried out by Felix Benjamin Schäfer at the
Physikalisches Institut of the University of Heidelberg
under the supervision of
Dr. Kai Schweda

Abstract

This thesis analyzes the effects of polarization in the decay $D^*(2010)^+ \rightarrow D^0(\pi^+K^-) + \pi^+$ and their influence on cross section measurements at ALICE at the LHC. The decay kinematics are studied and anisotropic spatial distributions of decay daughters for polarized D^{*+} mesons are derived. The influence of these altered spatial distributions on detector acceptance and the correlated uncertainty of the cross section analyses is discussed for a D^{*+} meson decaying at rest. A simulation macro implementing anisotropic decays is presented in order to calculate these effects for general D^{*+} momenta in the helicity and Collins-Soper reference frames. A strong influence of polarization on the acceptance due to kinematic cuts on the decay daughters in η and p_T is found for D^{*+} mesons at low transverse momenta. The effect diminishes for transverse momenta above 2 to 4 GeV/c, determined mainly by the p_T cut on the low momentum soft pion from the primary decay. As all D^{*+} cross section measurements in lead-lead collisions by the ALICE collaboration presently start just above the momentum range where the acceptance is influenced by polarization, the uncertainty due to polarization is negligible for these measurements. In the analysis of proton-proton collisions, the cross section value in the transverse momentum bin [1, 2] GeV/c exhibits an uncertainty of ${}_{-5.6}^{+13.8}\%$ due to yet unknown polarization, leading to an uncertainty of the integrated cross section of ${}_{-2.5}^{+6.4}\%$, which is significant compared to the remaining statistical and systematic uncertainties.

Kurzfassung

In dieser Arbeit werden die Auswirkungen von Polarisation im Zerfall $D^*(2010)^+ \rightarrow D^0(\pi^+K^-) + \pi^+$ und deren Einfluss auf Messungen des Wirkungsquerschnitts im ALICE Detektor am LHC untersucht. Die Zerfallskinetik wird diskutiert und die anisotropen Winkelverteilungen der Zerfallsprodukte polarisierter D^* Mesonen hergeleitet. Der Einfluss dieser veränderten räumlichen Verteilungen auf die Detektorakzeptanz und die damit verbundene Unbestimmtheit des Wirkungsquerschnitts wird für in Ruhe zerfallende D^{*+} Mesonen bestimmt. Es wird eine Simulation zur Untersuchung dieser Effekte für beliebige Impulse des Mutterteilchens vorgestellt, die anisotrope Zerfälle implementiert und die Betrachtung von Polarisation in den Helizitäts- und Collins-Soper-Bezugssystemen ermöglicht.

Es ergeben sich wesentliche Auswirkungen von Polarisation auf die Akzeptanz aufgrund der Grenzen der kinematischen Parameter η und p_T der Zerfallsprodukte von D^{*+} Mesonen mit niedrigem Transversalimpuls. Der Einfluss verschwindet für Transversalimpulse oberhalb von 2 bis 4 GeV/c, je nach Wahl der p_T Schwelle für das Pion mit geringem Impuls aus dem ersten Zerfall. Da alle bisherigen Messungen des Wirkungsquerschnitts der ALICE Kollaboration in Blei-Blei Kollisionen etwas oberhalb des Impulsbereichs der Polarisationseffekte beginnen, ist hier die Unbestimmtheit durch Polarisation zu vernachlässigen. In der Analyse von Proton-Proton Kollisionen hingegen ergibt sich im Bereich zwischen 1 und 2 GeV/c die Unbestimmtheit des differentiellen Wirkungsquerschnitts zu ${}_{-5.6}^{+13.8}\%$ aufgrund des unbekanntem Polarisationeszustandes. Dies führt zu einer Unbestimmtheit des totalen Wirkungsquerschnitts von ${}_{-2.5}^{+6.4}\%$, die im Vergleich zu den übrigen systematischen und statistischen Fehlern signifikant ist.

Contents

1	Introduction	1
2	ALICE at the LHC	3
3	Theoretical background	5
3.1	Decay kinematics	5
3.2	Angular distributions of polarized D^* decays	6
3.3	Analysis cuts and detector acceptance	8
3.4	Determination of cross sections from raw yields	11
4	Monte Carlo simulations	13
4.1	Decay routine	13
4.2	Simulation concept	14
5	Results	17
5.1	Spatial distribution of decay products in D^* rest frame	17
5.2	Acceptance effects due to η -cut	21
5.2.1	Effect of increasing $p_T(D^*)$, $y(D^*) = 0$	21
5.2.2	Effect of flat distribution in $ y(D^*) < 0.5$	25
5.2.3	Acceptance effect for increasing p_T	27
5.3	Acceptance effects due to p_T -cut	29
5.3.1	Shape of p_T -spectra of decay products	29
5.3.2	Transverse momentum spectra of soft pion for increasing $p_T(D^*)$	32
5.3.3	Acceptance effects	34
5.4	Combined acceptance effects and implication on cross section measurements	36
5.4.1	Polarization uncertainty of D^* cross section measurements in pp collisions	38
5.5	Discussion of errors	41
6	Conclusion	43
A	Figures of polarization effects in Collins-Soper frame	47
B	Tabulated values of relative acceptance for different p_T cuts	53
C	Influence of p_T-cuts on secondary pions and kaons	57

1 Introduction

When studying particle decays, one often considers the angular distributions of the decay products to be isotropic in the rest frame of the mother particle. This assumption breaks down when looking at certain decays of polarized particles.

The polarization of a particle is generally defined by the relative orientation between its total angular momentum vector \vec{J} and a quantization axis \vec{e}_z . In certain decay channels, polarized states of the decaying particle can lead to anisotropic angular distributions of the decay products.

In the decay channel $D^*(2010)^+ \rightarrow D^0 + \pi^+$, the decay products show a relative orbital angular momentum and are therefore distributed according to spherical harmonics for pure polarization states. This leads to a higher probability of emission parallel or perpendicular to the quantization axis, depending on the specific $D^*(2010)^+$ (from now on: D^{*+}) polarization.

The ALICE (A Large Ion Collider Experiment) central barrel detectors are geometrically limited to detect particles with polar angle $\frac{\pi}{4} < \theta < \frac{3\pi}{4}$ with respect to the beam axis. The D^{*+} -meson can only be reconstructed if all decay products are within this detection range. If these are now distributed in such a way that they have a higher probability of being outside this range than in an isotropic distribution, the probability of detection and thus detector acceptance will be lower.

When measuring the cross section of a particle, the raw measured particle yields are corrected with the detector acceptance α and reconstruction efficiencies ϵ of the decay products. This factor, often abbreviated by $\alpha \times \epsilon$ or $Acc \times \epsilon$, is obtained in full detector Monte Carlo simulations with an event generator. None of the existing generators implement anisotropic angular distributions for decays of polarized D^{*+} -mesons.

The polarization of D^{*+} is currently unknown at LHC energies. This leads to an uncertainty in the calculation of $\alpha \times \epsilon$ which directly implies a corresponding systematic uncertainty in the calculation of the cross section. This has not been taken into account in previous analyses of the D^{*+} cross section.

In this bachelor thesis, the kinematics of the decay $D^*(2010)^+ \rightarrow D^0 + \pi^+$ for polarized D^{*+} -mesons are studied. The resulting acceptance effects are determined in a Monte Carlo simulation and applied to existing cross section measurements in proton-proton and lead-lead collisions. We will find that polarization effects can have a significant impact on these measurements and need to be considered as an additional systematic uncertainty in future analyses.

The thesis is organized as follows: After a brief introduction to the context of this thesis within ALICE at the LHC in chapter 2, chapter 3 outlines the decay kinematics, the concept of polarization and the role of the detector acceptance in cross section measurements. The Monte Carlo simulation routine implemented to study the decay is described in chapter 4. In chapter 5, the kinematics of polarized D^* decays are analyzed step by step in order to understand the resulting acceptance effects and their influence on the measured cross sections.

2 ALICE at the LHC

The Large Hadron Collider (LHC) is a circular particle accelerator constructed and operated by the European Organization for Nuclear Research (CERN) near Geneva, Switzerland. Built in a tunnel with a circumference of 27 km, it is the largest, highest-energy and highest-luminosity hadron accelerator in the world, currently colliding protons with a center-of-mass energy of $\sqrt{s} = 7$ TeV and lead nuclei with $\sqrt{s_{NN}} = 2.76$ TeV.

Out of the four main experiments at the LHC, the ATLAS, CMS and LHCb collaborations focus on proton-proton (pp) collisions while the ALICE (A Large Ion Collider Experiment) collaboration specializes in the study of the collisions of lead nuclei (Pb-Pb). In these collisions with high particle multiplicities, extremely high energy densities and temperatures, the formation of a deconfined phase of strongly-interacting matter, the Quark-Gluon-Plasma (QGP), is expected to be formed by Quantum Chromodynamics (see e.g. [1]). One of the main goals of the experiment is the analysis of the properties of this plasma, which had fundamental implications on the detector design.

The ALICE detector consists of a forward muon spectrometer, a number of forward detectors for triggering and event characterization and various detectors in the cylindrical central barrel for mid-rapidity particle reconstruction [2]. These include going outward from beam:

- Inner Tracking System (ITS), a six layer silicon detector for primary and secondary vertex reconstruction, measurement of the impact parameter of tracks and particle identification (PID) of low momentum (< 200 MeV¹) particles.
- Time-Projection Chamber (TPC), a gas detector with 85 m³ active volume for track reconstruction and p_T determination as well as PID by measuring the specific energy deposit dE/dx .
- Transition Radiation Detector (TRD), a detector with the primary objective of electron/pion separation above 1 GeV via measurement of the characteristic transition radiation of electrons passing through a radiator.
- Time-of-Flight (TOF), measuring the time of flight of particles from the interaction point, mainly used for separation of pions, kaons and protons in combination with TPC tracking in the intermediate momentum range.

¹Natural units will be used in this thesis, setting $\hbar = c = 1$.

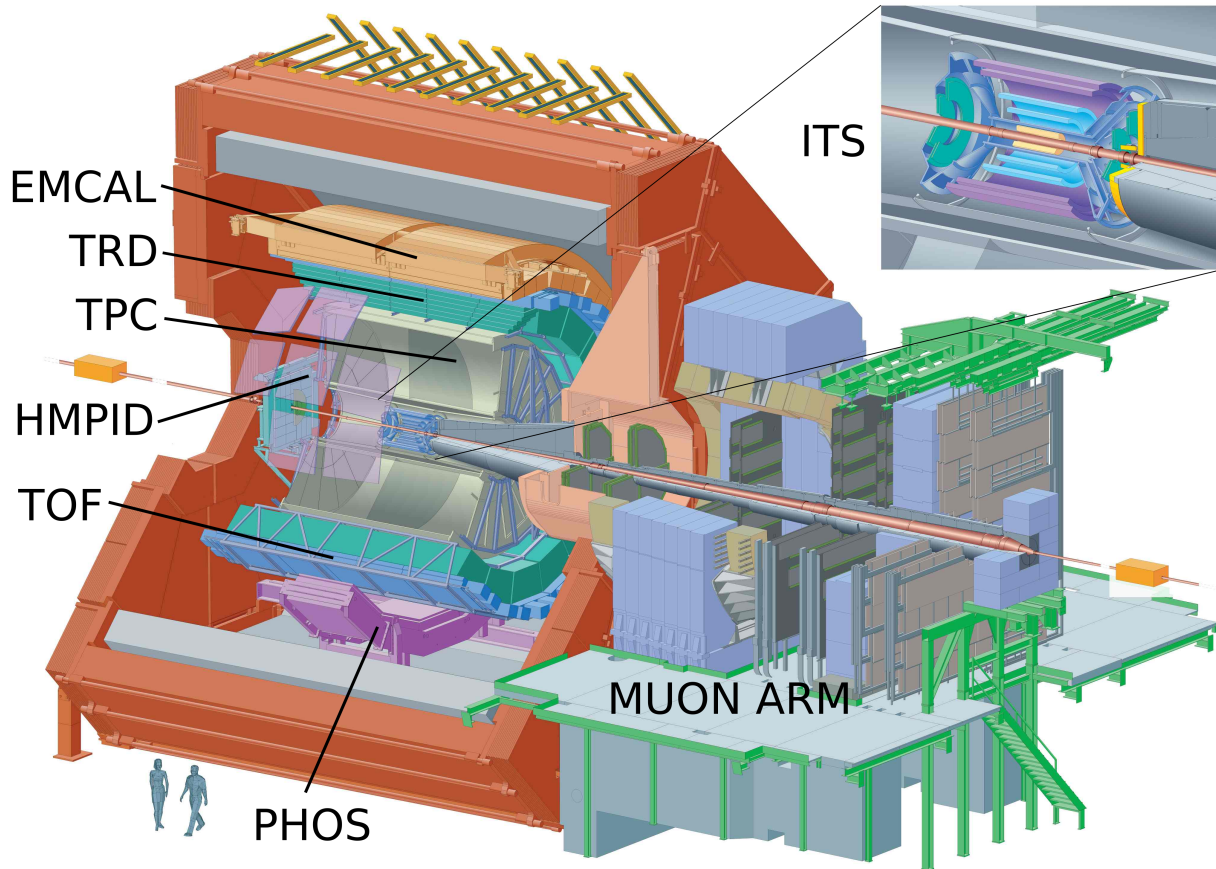


Figure 2.1: ALICE schematic layout [3]

With this setup, the ALICE central barrel detector has the capability to separate tracks at high multiplicities, measure in a wide momentum range over three orders of magnitude (few 10 MeV to > 100 GeV) and provide PID over a large part of this range, making it unique for the analysis of Pb-Pb collisions and the Quark-Gluon-Plasma.

Gluons and quarks produced at the initial stage of the collision suffer energy loss when traversing the QGP. This energy loss is measured by the nuclear modification factor R_{AA} , which characterizes the suppression of particle production in Pb-Pb collisions compared to a pp reference. This pp reference is the particle production measured in proton-proton collisions scaled with the average number of binary nucleon-nucleon collisions occurring in Pb-Pb collisions. In order to understand the processes underlying this energy loss, the nuclear modification factors of different hadronic states are compared to study mass and color charge dependencies. Due to their higher mass, hadrons containing heavy quarks have a shorter formation time than light-quark hadrons. A difference in suppression between these particles can therefore be an indicator for other processes determined by in-medium hadron formation and dissociation [4, 5]. The measurement of charmed D-mesons and their suppression therefore plays an important role in probing the QGP.

3 Theoretical background

3.1 Decay kinematics

In ALICE, the D^{*+} meson is reconstructed in the following decay channel:

$$D^{*+} \xrightarrow{(1)} D^0 + \pi^+ \xrightarrow{(2)} 2\pi^+ + K^- \quad (1)$$

	D^{*+}	π^+	D^0	K^-
m_0 [GeV]	2.010	0.140	1.865	0.494

Table 3.1: Rest masses of particles in observed decay channel [6]. Values rounded to full MeV, errors negligible for this consideration.

The same holds for D^{*-} with the corresponding anti-particles as decay products, as do all the following considerations. In previous cross section measurements, the raw yields of D^{*+} and antiparticle were aggregated into one analysis [7]. Therefore, I will refer to the “ D^* meson” whenever it is not determined by the specific decay channel.

The decay kinematics of the primary decay $D^{*+} \rightarrow D^0 + \pi^+$ play an essential role in this polarization analysis. Due to the small mass difference $\Delta m = m(D^{*+}) - m(D^0) - m(\pi^+) \approx 6$ MeV, the decay daughters have small momenta in the D^* rest frame. In this frame, the magnitude of the momentum vector in a two-body decay with mass difference Δm and daughter particle masses $m_{1,2}$ is generally given by:

$$|\vec{p}| = \frac{\sqrt{\Delta m(\Delta m + 2m_1)(\Delta m + 2m_2)(\Delta m + 2(m_1 + m_2))}}{2(\Delta m + m_2 + m_1)} \quad (2)$$

With the particle data group (PDG) [6] masses, this yields $|\vec{p}_{1,2}| \approx 39$ MeV. Due to momentum conservation, the particles are emitted back-to-back ($\vec{p}_1 = -\vec{p}_2$) in the D^* rest frame. In decays of particles with spin $s = 0$, all directions of emission have the same probability and the angular distributions are isotropic. In chapter 3.2, we will see that decays of polarized $s = 1$ particles can show anisotropic distributions of decay daughters.

For D^* mesons with non-zero momentum, the reference frame of our detector (from now on: lab frame) will differ from the D^* rest frame (from now on: rest frame) and we have to consider the Lorentz transformation. In order to understand the implications on the kinematics, we will now study the one-dimensional case where π^+ and D^0 are emitted along the axis defined by the D^* momentum vector. The momentum in the lab frame p' can then be obtained by

$$p' = \gamma p + \gamma \beta \sqrt{p^2 + m^2} \quad (3)$$

with daughter particle momentum in the rest frame p , mass m and the Lorentz factor γ and relativistic velocity β of the decayed particle. We consider a D^* meson with $p = 2.5$ GeV in the lab frame. For the two cases of emission a) D^0 in direction of D^* , π^+ in the opposite direction and b) vice versa we get

- a) $(p'(\pi^+), p'(D^0)) \approx (119 \text{ MeV}, 2381 \text{ MeV})$
 b) $(p'(\pi^+), p'(D^0)) \approx (243 \text{ MeV}, 2257 \text{ MeV})$.

Due to the much larger mass, the D^0 carries a far greater part of the mother particle momentum than the pion. The disproportional mass ratio and the low particle momentum in the rest frame lead to the pion obtaining low momentum in the lab frame, which is therefore often called the “soft pion” in this decay. In chapter 5.3.1, we will see that this holds for the universal 3-dimensional case, where the direction of the D^0 differs little from the original D^* momentum.

If we restrict our decay to the plane perpendicular to the beam axis, we can predict the expected transverse momentum spectra of the decay daughters. The soft pion obtains maximum p_T when being emitted parallel to the D^* flight direction and lowest p_T in the antiparallel case. These are the boundaries of our spectrum. For any other direction of emission, we get a p_T within this range and therefore expect a continuous spectrum with sharp flanks in case of high statistics. In the pp cross section analysis of the D^* meson [7], a minimum p_T of 80 MeV is required for the soft pion (see chapter 3.3). This corresponds to the upper boundary of an expected soft pion spectrum of a D^* meson with $p_T \approx 550$ MeV. This will be the low- p_T limit of detecting a D^* meson. The exact shape of the continuum will depend on the angular distribution of the decay daughter.

Due to the higher mass difference Δm in the secondary decay $D^0 \rightarrow \pi^+ + K^-$, the secondary pion and kaon exhibit a momentum of $|\vec{p}| \approx 861$ MeV in the D^0 rest frame. In the case of forward emission, this leads to particles with much larger momenta than the initial D^* particle. It also leads to a broader p_T spectrum in the lab frame than those of soft pion and D^0 .

3.2 Angular distributions of polarized D^* decays

We will now analyze the configuration of angular momentum in the observed decay channel.

	D^{*+}	π^+	D^0	K^-
J^P	1^-	0^-	0^-	0^-

Table 3.2: Total angular momentum J and parity P of particles in observed decay channel[6].

All particles of the secondary decay $D^0 \rightarrow \pi^+ + K^-$ have spin $s = 0$. Therefore, the secondary pion π_2^+ and kaon K^- are distributed isotropically in the D^0 rest frame. The mother particle D^* of the primary decay carries spin $s = 1$. Since the products of this strong decay carry no spin and both have parity -1 , they must have a relative angular momentum with quantum number $l = 1$ due to the conservation of total angular momentum J and parity P in the strong interaction.

In general, the spin vector \vec{S} of the D^* meson can have any orientation with respect to an axis of quantization \vec{e}_z expressed in spherical coordinates (θ, ϕ) . The projection S_z will then be $S_z = |\vec{S}| \cdot \cos \theta$. Due to the conservation of J_z , the projection of relative angular momentum of

the daughter particles will be $L_z = S_z$.

We can express the states of mother and daughter particles in the eigenbasis $|j, m_j\rangle$ of the total angular momentum operator \hat{J} :

$$|D^{*+}\rangle = \sum_{m_s=-1,0,1} C_{m_s} \cdot |1, m_s\rangle. \quad (4)$$

$$|\pi^+ D^0\rangle = \sum_{m_l=-1,0,1} C_{m_l} \cdot |1, m_l\rangle. \quad (5)$$

$$\text{with } \langle \pi^+ D^0 | \hat{J}_z | \pi^+ D^0 \rangle = \langle D^{*+} | \hat{J}_z | D^{*+} \rangle. \quad (6)$$

In position-space, we obtain the wave function of the decay daughters in spherical coordinates

$$\begin{aligned} \Psi(\theta, \phi) &= \langle \theta, \phi | \pi^+ D^0 \rangle = \sum_{m_l=-1,0,1} C_{m_l} \cdot \langle \theta, \phi | 1, m_l \rangle \\ &= \sum_{m_l=-1,0,1} C_{m_l} \cdot Y_{1m_l} \end{aligned} \quad (7)$$

with the spherical harmonics Y_{lm_l} .

The D^{*+} is considered to be polarized if it is in a pure state $|1, \pm 1\rangle$ (transverse) or $|1, 0\rangle$ (longitudinal). This rather counterintuitive definition originates from the polarization definition of a photon, where the spin is aligned along its momentum while the electromagnetic field oscillates in the plane perpendicular to the direction of motion.[8]

In the case of a polarized D^* , the decay daughters will be in the states

$$|D^{*+}\rangle = |1, \pm 1\rangle \quad \rightarrow \quad |\pi^+ D^0\rangle = |1, \pm 1\rangle \quad \text{for transverse polarization,} \quad (8)$$

$$|D^{*+}\rangle = |1, 0\rangle \quad \rightarrow \quad |\pi^+ D^0\rangle = |1, 0\rangle \quad \text{for longitudinal polarization.} \quad (9)$$

The emission probability densities of the decay products will be

$$\rho(\theta, \phi, m_l = m_s = \pm 1) = |\Psi|^2 = |C_{\pm 1}|^2 \cdot |Y_{1\pm 1}|^2 = \frac{3}{8\pi} \sin^2 \theta \quad (10)$$

for transverse polarization and

$$\rho(\theta, \phi, m_l = m_s = 0) = |\Psi|^2 = |C_0|^2 \cdot |Y_{10}|^2 = \frac{3}{4\pi} \cos^2 \theta \quad (11)$$

for longitudinal polarization, after normalization.

The isotropic case leads to

$$\rho(\theta, \phi) = |\Psi|^2 = \frac{1}{4\pi}. \quad (12)$$

In general, the D^* will be in a mixed state and the emission probability will be

$$|\Psi(\theta, \phi)|^2 = \left| \sum_{m_l=-1,0,1} C_{m_l} \cdot Y_{1m_l} \right|^2 \quad (13)$$

with coefficients C_{m_l} determining the contribution of the different states. In this analysis, we will focus on pure states.

The angular emission probability densities obtained in the rest frame will generally look different in the lab frame due to the Lorentz transformation. This has an important implication on the acceptance effects and will be studied in chapter 5.2.1.

The choice of the quantization axis \vec{e}_z strongly influences the resulting angular distributions in the lab frame. As in previous studies of quarkonium polarization [8], two reference frames will be considered:

- **Helicity frame:** quantization axis $\vec{e}_z = \vec{p}(D^*)$ of the decaying particle, corresponding to the direction of the Lorentz boost between lab and rest frame. The angular distributions will therefore be rotated in the lab frame depending on the direction of D^* momentum.
- **Collins-Soper frame:** quantization axis \vec{e}_z is the bisector of the angle between one beam and the opposite of the other beam [9]. As the crossing angle of beams in ALICE is of the order of 10^{-4} rad [10], this is the beam direction and thus z-axis in the lab frame in good approximation. For D^* mesons polarized in this frame, the angular distributions will be independent of the direction of D^* momentum.

The D^* polarization in both of these reference frames is currently unknown. We will study transverse and longitudinal polarization states for both reference frames as extreme cases in terms of the acceptance effect.

3.3 Analysis cuts and detector acceptance

Due to its geometry, the ALICE central barrel detectors can reconstruct particles with pseudorapidity $|\eta| < 0.8$, approximately corresponding to polar angles between $\frac{\pi}{4} < \theta < \frac{3\pi}{4}$ with respect to the beam axis in the coordinate system defined in figure 3.1.

In the previous D^* cross section analyses [7, 11, 12], only daughter particles within this phase-space region were considered. In addition, a minimum p_T of the decay daughters was required in order to reduce background and avoid unsatisfactory track reconstruction efficiencies at low momenta, where the trajectories of charged particles are curved in the magnetic field of the detector in such a way that they don't reach the TPC needed for the reconstruction.

These selection criteria (from now on referred to as “cuts”) reduce the fraction of produced particles observed in the detector. The cuts applied in the D^* cross section analyses are shown in table 3.3.

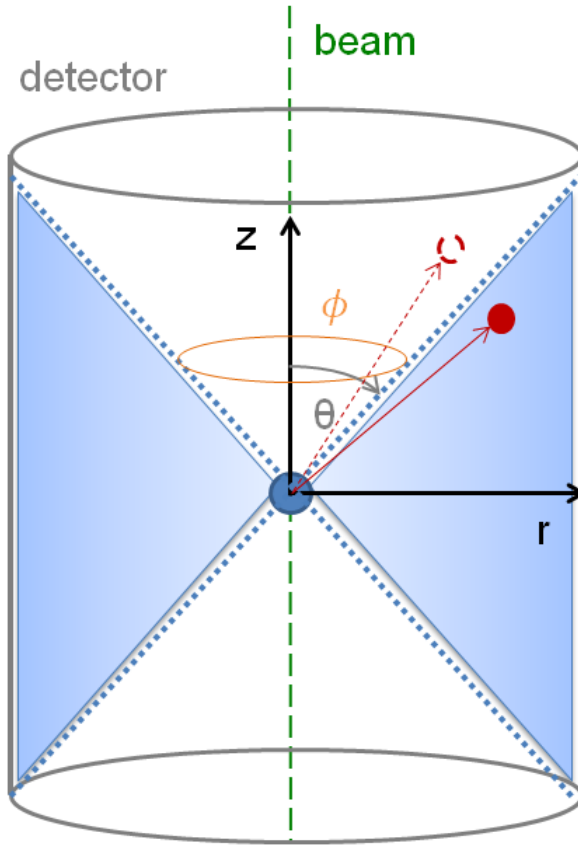


Figure 3.1: Laboratory reference frame and angular acceptance range of central barrel detectors.

Collision	$ \eta _{max}(\pi_1^+, \pi_2^+, K^-)$	$p_{T,min}(\pi_1^+)$ (MeV)	$p_{T,min}(\pi_2^+, K^-)$ (MeV)
$pp, \sqrt{s} = 7$ TeV	0.8	80	400
Pb-Pb 2010, $\sqrt{s} = 2.76$ TeV (centrality 0 – 20%)	0.8	200	700
Pb-Pb 2010, $\sqrt{s} = 2.76$ TeV (centrality 40 – 80%)	0.8	100	500
Pb-Pb 2011, $\sqrt{s} = 2.76$ TeV (centrality 0 – 7.5%)	0.8	100	500

Table 3.3: Daughter particle selection criteria for the reconstruction of D^* -candidates in previous D^* cross section analyses [7, 11, 12]. The p_T cuts on secondary pion π_2^+ and K^- were set p_T dependent in the analyses. The given value represents the lowest p_T cut applied. See appendix C for further discussion.

The acceptance α of a detector is defined by

$$\alpha(p_T, \eta) = \frac{d^2 N_{\text{inside cuts}}}{dp_T d\eta} / \frac{d^2 N_{\text{total}}}{dp_T d\eta} \quad (14)$$

with $N_{\text{inside cuts}}$ being the number of particles which are produced within the kinematic cuts and N_{total} being the total number of particles produced. In our case, N_{total} is the number of D^* particles produced within the rapidity interval considered for the analysis (see section 4.2). The acceptance is determined by the detector setup and the chosen kinematic cuts. It is dependent on the transverse particle momentum p_T and pseudorapidity η and therefore also on the polar angle θ . Due to the azimuthal symmetry of the central barrel detector, the acceptance is usually independent of ϕ in this definition.

In order to understand the effects of polarization due to different η - and p_T -cuts, a separate study will be conducted for each of these cuts. The acceptance due to η -cuts (no p_T -cuts) will be labeled α_η and the inverse case α_{p_T} . The total acceptance effect due to the combination of both cuts will be called α .

For easier comparison, the relative acceptance $\alpha_{rel}^{t,l} \equiv \alpha^{t,l}/\alpha^0$ is often calculated, showing the ratio of acceptance for the polarized to the unpolarized (isotropic) case. A ratio different from unity directly represents the size of the systematical uncertainty when anisotropic distributions of decay daughters due to polarization are not taken into account.

We can now calculate the expected acceptance ratios between different polarization cases for a quasi-resting D^* meson with $\vec{p}(D^*) \parallel \vec{e}_z$. In this case, the angular distributions in Collins-Soper and helicity frames coincide.

The acceptance effect due to the limited angular coverage can be calculated by integrating the probability density over the acceptance range:

$$\alpha_\eta^0 = \int_0^{2\pi} d\phi \int_{\theta(\eta=-0.8)}^{\theta(\eta=0.8)} \rho(\theta, \phi) \sin(\theta) d\theta = 0.649 \quad (\text{no polarization})$$

with the integral limits $\theta_{1,2}(\eta) = 2 \arctan(e^{-\eta})$. This leads to

- a) $\alpha_{\eta,1}^t = 0.836$ (transverse polarization)
- b) $\alpha_{\eta,1}^l = 0.274$ (longitudinal polarization).

This is the acceptance of the primary decay. Since we observe the soft pion from the primary decay and the products of the the isotropic secondary decay $D^0 \rightarrow \pi^+ + K^-$, we have to multiply this acceptance with the probability of detecting an isotropically emitted particle (kaon/pion). This yields

- a) $\alpha_\eta^t = \alpha_{\eta,1}^t \cdot 0.649 = 0.543$ (transverse polarization)
- b) $\alpha_\eta^l = \alpha_{\eta,1}^l \cdot 0.649 = 0.178$ (longitudinal polarization)

The resulting acceptance ratios

$$\text{a) } \alpha_{\eta,rel}^t = \frac{\alpha_{\eta}^t}{\alpha_{\eta}^0} = 0.424 \quad (\text{transverse polarization})$$

$$\text{b) } \alpha_{\eta,rel}^l = \frac{\alpha_{\eta}^l}{\alpha_{\eta}^0} = 1.288 \quad (\text{longitudinal polarization})$$

are equal for both primary and secondary decay and significantly differ from unity, which motivates further investigation. In chapter 5.1, the results of the Monte Carlo simulation will be compared to these values.

When calculating acceptance values $\alpha = N_{\text{inside cuts}}/N_{\text{total}}$ for a certain region of phase space, the corresponding errors cannot be obtained by Gaussian error propagation. Since $N_{\text{inside cuts}}$ is a subset of $N_{\text{total}} = N_{\text{inside cuts}} + N_{\text{outside cuts}}$, these two quantities are correlated. It is therefore necessary to apply the concept of binomial errors, reflecting the fact that an acceptance effect due to a cut can be considered a binomial process (particle either inside acceptance range or outside acceptance range). The statistical error in this case is given by

$$\Delta\alpha = \sqrt{\frac{\alpha(1-\alpha)}{N_{\text{total}}}} \quad [13]. \quad (15)$$

3.4 Determination of cross sections from raw yields

In order to determine the raw production yields, the invariant mass difference of all three D^* -candidate decay tracks and the reconstructed D^0 from the primary decay is analyzed for specific p_T -ranges [7]. The invariant mass peak is fitted by a Gaussian and the raw yield is calculated after background subtraction. The production cross section is then derived from the raw yield:

$$\left. \frac{d\sigma^{D^{*+}}}{dp_T} \right|_{|y|<0.5}^0 = \frac{1}{2} \frac{1}{\Delta p_T} \frac{f_{\text{prompt}}(p_T) \cdot N_{\text{raw}}^{D^*}(p_T)}{(\alpha \times \epsilon)_{\text{prompt}}^0(p_T) \cdot \text{BR} \cdot L_{\text{int}}} \quad (16)$$

where the factor 1/2 accounts for the summation of D^{*+} and D^{*-} raw yield, Δp_T corresponds to the width of the respective analysis interval. BR is the total branching ratio of the decay channels and L_{int} the integrated luminosity of the data sample. f_{prompt} is the fraction of (“prompt”) D^* mesons produced in the primary collision and $(\alpha \times \epsilon)_{\text{prompt}}^0$ the corresponding acceptance times efficiency of prompt mesons when assuming isotropic distributions of decay daughters. The indices $0,t,l$ in certain quantities indicate the different cases of no polarization, transverse polarization and longitudinal polarization.

$(\alpha \times \epsilon)$ accounts for the acceptance α defined by the kinematic selection cuts times the D^* reconstruction efficiencies ϵ after selection cuts used in the analysis. They are calculated in a full Monte Carlo detector simulation. These simulations generate events using the PYTHIA 6.4.21 generator [14] and propagate the produced particles and their decay products through the detector, providing full event information. The decay routines of these generators do not implement anisotropic decays of polarized D^* mesons. The resulting acceptance times efficiency is therefore incorrect in the case of polarized D^* mesons. The goal of this thesis is to quantify

these differences in acceptance due to different polarization states.

We now assume the acceptance due to kinematic cuts to be independent of the reconstruction efficiencies within a certain region Δp_T .

We can then write

$$(\alpha \times \epsilon)_{prompt}^0 = \epsilon_{prompt} \cdot \alpha^0 \quad (17)$$

for the isotropic case. One obtains

$$(\alpha \times \epsilon)_{prompt}^{t,l} \equiv \epsilon_{prompt} \cdot \alpha^{t,l} = (\alpha \times \epsilon)_{prompt}^0 \cdot \frac{\alpha^{t,l}}{\alpha^0}. \quad (18)$$

for the polarized case.

The cross sections can then be calculated by:

$$\left. \frac{d\sigma^{D^{+*}}}{dp_T} \right|_{|y|<0.5}^{t,l} = \left. \frac{d\sigma^{D^{+*}}}{dp_T} \right|_{|y|<0.5}^0 \cdot \frac{(\alpha \times \epsilon)_{prompt}^0}{(\alpha \times \epsilon)_{prompt}^{t,l}} = \left. \frac{d\sigma^{D^{+*}}}{dp_T} \right|_{|y|<0.5}^0 \cdot \frac{\alpha^0}{\alpha^{t,l}} = \left. \frac{d\sigma^{D^{+*}}}{dp_T} \right|_{|y|<0.5}^0 \cdot (\alpha_{rel}^{t,l})^{-1} \quad (19)$$

4 Monte Carlo simulations

The acceptance effects of polarized D^* -mesons were analyzed in a Monte Carlo (MC) simulation. A thorough search revealed that none of the typical simulation frameworks implements anisotropic angular distributions of polarized D^* -decays.

The ALICE collaboration uses the C++-based framework `AliRoot` for data analysis and simulations. The `AliRoot` class `AliDecayerPolarized` implements anisotropic decays of polarized quarkonia (J/Ψ , Ψ' , Υ , Υ') in dilepton decays. This class has already been used in analyses of the J/Ψ meson [15], providing an uncertainty due to polarization in the measurement of the the production cross section.

The `PYTHIA 6` [14] and `8` [16] frameworks are used in analyses for MC based event generation and decay simulations as plugins of `AliRoot`. They support no consideration of meson polarization. In `PYTHIA 8.145` (from now on: `PYTHIA`), it is however possible to overwrite the internal decay routine described in 4.1 with a so called `External Decayer` class for a specific particle. This path was chosen for the following analysis. The implemented class varies little from the `PYTHIA` decay routine. It merely implements an anisotropic distribution of decay daughters defined by a probability distribution function and takes care of transformations needed to realize the helicity frame. Depending on the form of the $(\alpha \times \epsilon)$ -simulation in the D^* -analysis, both of these approaches can easily be implemented into the existing frameworks.

4.1 Decay routine

Since anisotropic meson decays are not implemented in the `PYTHIA` framework, a separate decay routine had to be written as a plugin-class. Figure 4.1 describes the steps of the `PYTHIA` particle decay routine and the changes applied in my case.

In order to setup the external decay class to work with `PYTHIA`, the class needs to be written according to a template defined by the framework. It has to inherit from the class `PYTHIA::DecayHandler`. After instantiation, it is passed to the `PYTHIA` method `setDecayPtr()`. When using the `AliRoot` class `AliDecayerPythia8` as an interface to `PYTHIA 8`, one has to make sure to call the method `PYTHIA::hadronLevel.decays.init()`, responsible for setting the internal decay pointer to the user defined class, as it is not called by the `AliDecayerPythia8`-constructor.

Once set up, this expansion of the `PYTHIA` framework can easily be altered to investigate anisotropic decays of any particle with an arbitrary angular distribution of decay products. Nevertheless, one has to be careful when randomizing the spherical coordinate variables (θ, ϕ) . Due to the θ -dependency of the solid angle element $d\Omega = \sin(\theta)d\theta d\phi$, the probability density function $\rho(\theta)$ has to be weighted with $\sin(\theta)$.

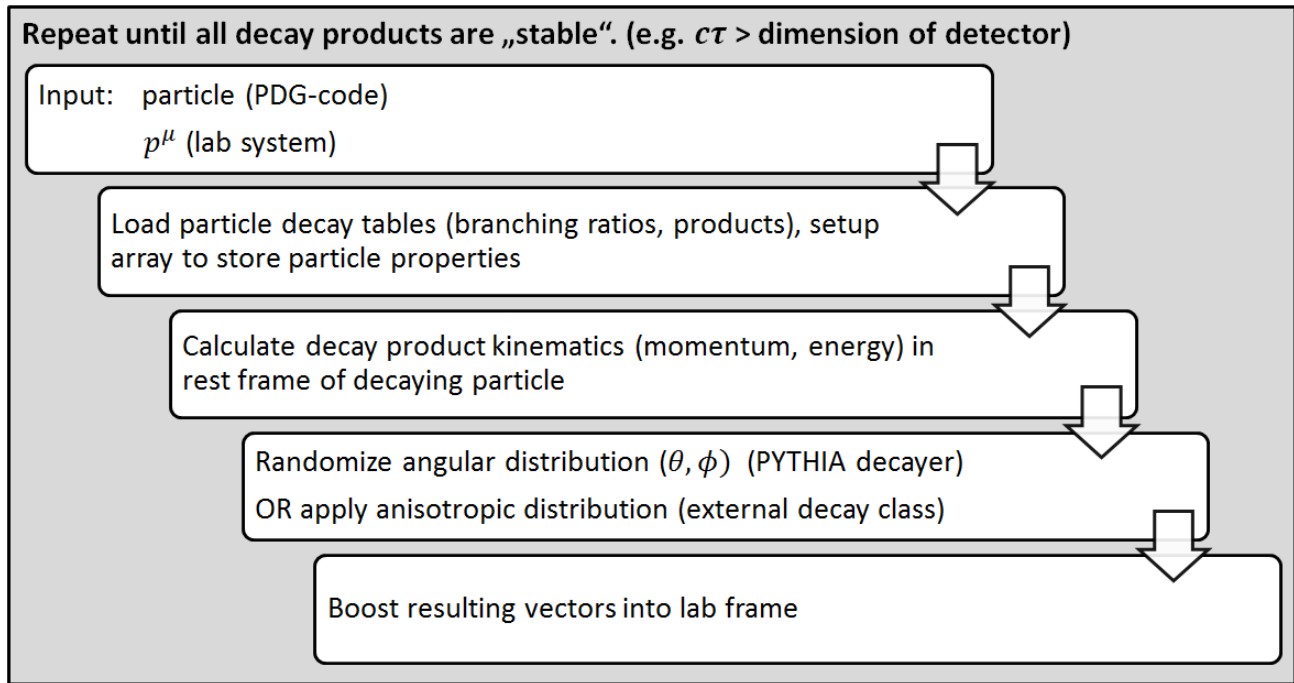


Figure 4.1: Decay routine of PYTHIA 8.

However, the implementation of non-uniform functions of angular distributions in the `External Decayer` slows down the decay routine considerably, as a new function object `TF1` is instantiated for every single decay. The simulation of a polarized decay takes about 100 times longer than for an isotropic distribution in PYTHIA. This leads to typical simulation times of ≈ 10 CPU minutes for 10^5 events. Depending on the implementation of the acceptance calculation of the analysis, this can be an argument against choosing the approach with the `External Decayer`.

4.2 Simulation concept

The implemented MC simulation creates D^* mesons at the initial vertex with transverse momentum and rapidity within specific ranges. The decay kinematics of these particles are then calculated by the PYTHIA decay scheme with the external decay class 4.1. The kinematics of the decay daughters are recorded and checked for compliance with the η and p_T cuts. By repeating this process 10^5 to 10^7 times, the acceptance can be calculated with a negligible error. The routine is repeated with identical parameters for the isotropic case, for transverse and for longitudinal polarization in order to calculate the relative acceptances. The full scheme is shown in figure 4.2.

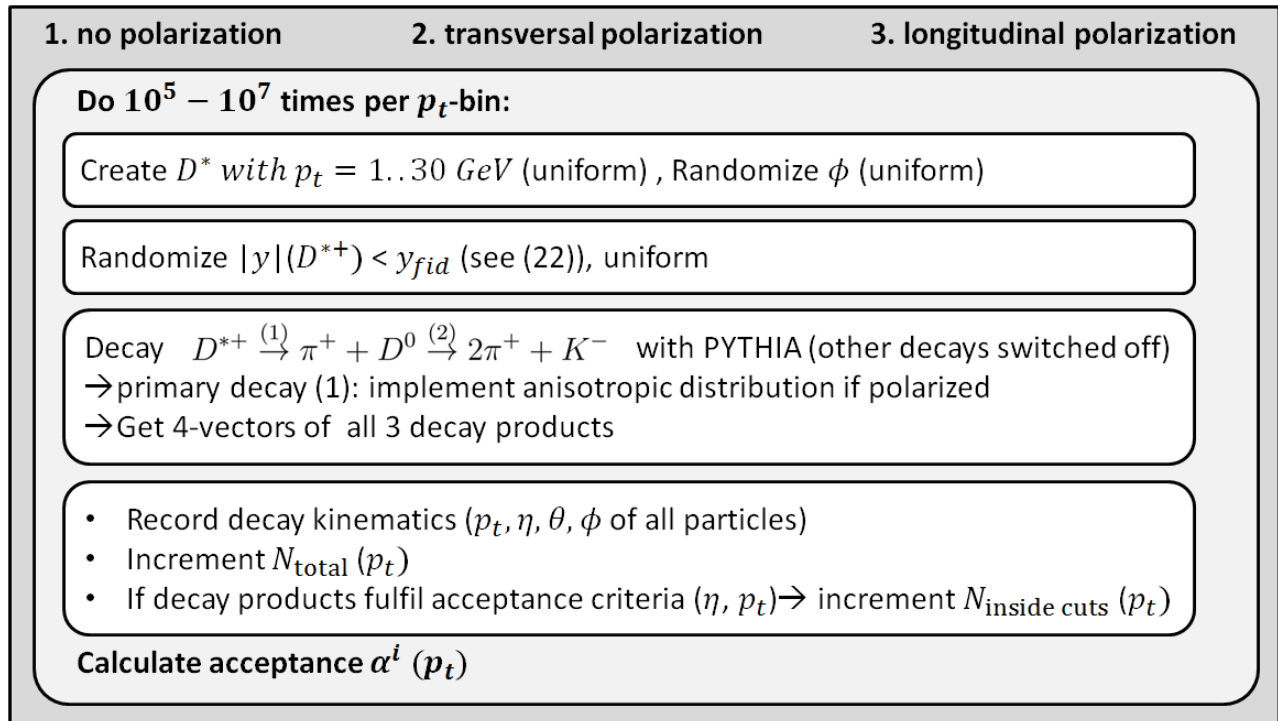


Figure 4.2: Scheme of MC simulation implemented for analysis of acceptance effect of polarization. The applied kinematic cuts are listed in table 3.3.

In the cross section analyses of D-mesons, only candidates within a so called fiducial acceptance interval $|y| < y_{fid}$ were taken into account. This interval is defined by

$$y_{fid} = \begin{cases} -\frac{0.2}{15}p_T^2 + \frac{1.9}{15}p_T + 0.5 & \text{for } p_T < 5 \text{ GeV} \\ 0.8 & \text{for } p_T \geq 5 \text{ GeV} \end{cases} \quad [7] \quad (20)$$

rising smoothly from $y = 0.5$ to $y = 0.8$ at 5 GeV in order to enhance statistics for higher p_T . As the y -distributions of D*-mesons in this region are uniform within 1% [7], the cross sections could easily be rescaled to the region $|y| < 0.5$. In order to be able to directly compare our results to this analysis, the D*-mesons were produced in MC according to this distribution in the simulation.

We will see that $10^5 - 10^7$ events are required to study the decay kinematics and acceptance effects for a specific D* momentum with sufficient statistics. When calculating acceptance effects for a range of D* transverse momenta, this number of events has to be calculated for every p_T bin, potentially leading to simulation times of several hundred CPU hours. The calculations were therefore performed on the batch farm of the working group, which consists of around 200 CPUs and is capable of parallel computing.

5 Results

In order to understand the results of the acceptance simulation, we will first study the decay kinematics for a quasi-resting D^* meson in chapter 5.1, moving on to more general initial D^* momenta and directions in sections 5.2.1 and 5.2.2. A separate study of acceptance effects due to the η -cuts (chapter 5.2) and the p_T -cuts (chapter 5.3) will be performed, culminating in the study of the combined cross section uncertainty in chapter 5.4. In chapter 5.5, the errors and the influence of the number of simulated events on the results are discussed.

To facilitate the description, most plots will only be shown in the helicity frame (“HX”). While the choice of reference frame will have a substantial impact on the acceptance effect, its explanation does not differ for the two frames. The corresponding figures in the Collins-Soper frame (“CS”) will be shown in appendix A. The resulting acceptance effects for the cross section analyses will be presented in chapter 5.4.

Most figures will feature a three-column layout, showing a certain quantity for the case of no polarization (left), transverse (middle) and longitudinal (right) polarization in order to compare the different cases. The left column represents the standard PYTHIA implementation of the decay while the other columns show the results of the external implementation of anisotropic decays. When the differences between distributions of certain quantities are hard to distinguish, ratios of distributions in the polarized case and the isotropic case are shown. In this case, a gray line indicating unity is shown to visualize the deviation from 1. The current reference frame is marked in the top left corner of each figure with the abbreviations “HX” (helicity frame) and “CS” (Collins-Soper frame).

5.1 Spatial distribution of decay products in D^* rest frame

The spatial distributions of the D^* meson decay products in its rest frame will be studied first. To achieve this, a small, non zero momentum of $|\vec{p}(D^*)| = 1 \text{ keV}$ ($\beta \approx 10^{-10}$) is applied in the simulation in order to define the quantization axis in the helicity frame. This state will be called “quasi-resting” from now on and can be considered as equivalent to a resting D^* . If we now set $\vec{p}(D^*) \parallel \vec{e}_z$, the D^* rest frame corresponds to the lab frame and Collins-Soper and helicity frames coincide. Figure 5.1 shows the spatial distributions obtained in this case.

As both products of the primary decay have the same spatial distribution (back-to-back emission) for a quasi-resting D^* , only the spatial distributions of the soft pion are shown. In the three-dimensional plots, one can recognize the lobe- and doughnut-shaped distributions known from the p-orbitals of hydrogen (squared spherical harmonics). The coordinate system for these representations is defined in figure 3.1. The deficiency of counts in the region $\theta \approx 0$ is due to binning effects at the edge of the range (also observable in the θ -distributions) in combination with a display error in the class responsible for three-dimensional plotting (`TH3DHistPainter`). These representations should therefore be seen as a pure visualization of the effect rather than a physical result.

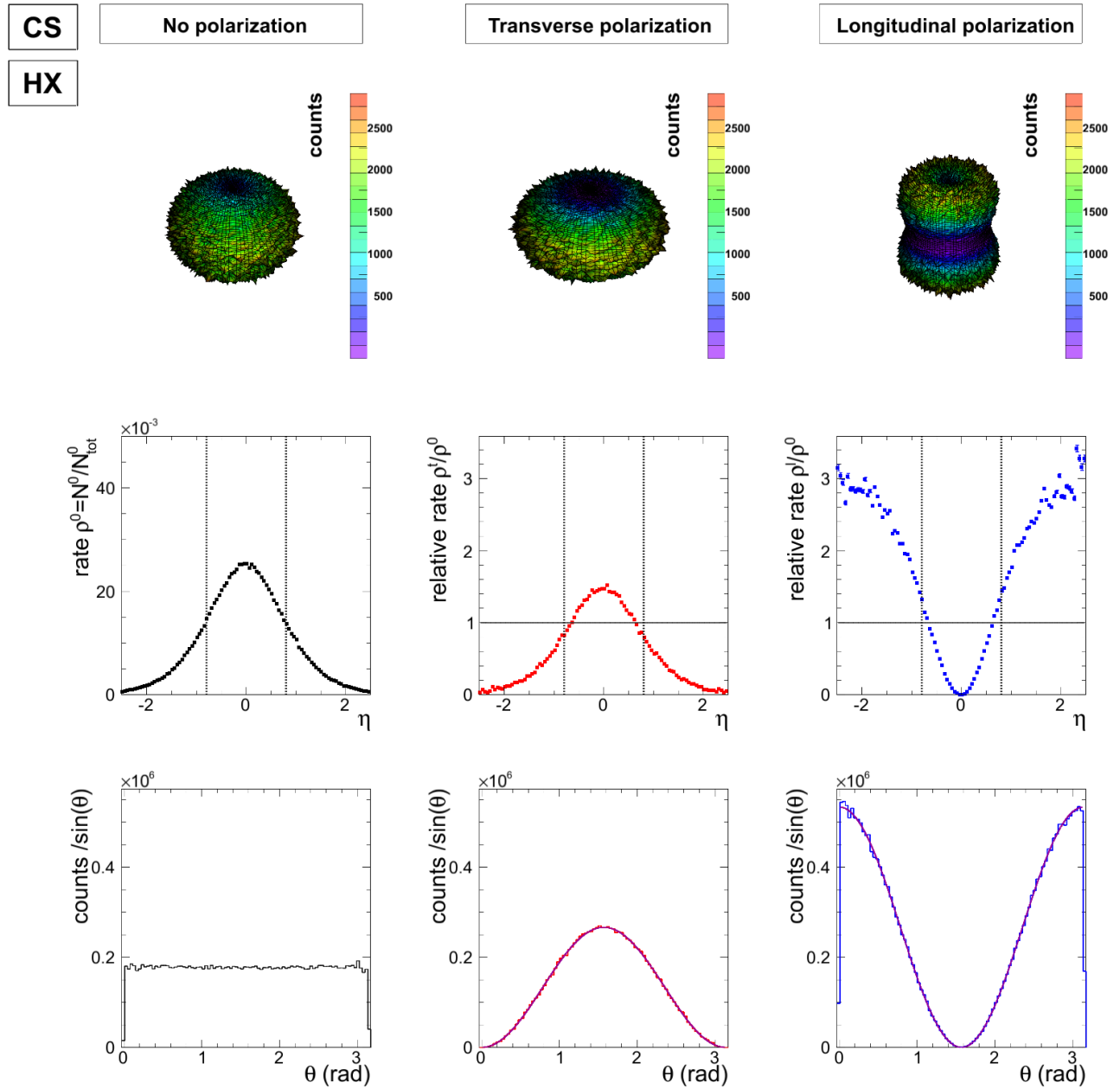


Figure 5.1: Spatial distribution of soft pion from D^* -decay for different polarization states with $|\vec{p}(D^*)| \approx 0$ GeV, $\vec{p}(D^*) \parallel \vec{e}_z$ for 10^7 events.

The θ -distributions illustrate the implemented anisotropic distributions $\rho^t(\theta) \propto \sin^2(\theta)$ and $\rho^l(\theta) \propto \cos^2(\theta)$, checked for consistency by fitting the obtained histograms with the corresponding functions. These histograms have been divided by $\sin(\theta)$ in order to take account of the solid angle element $d\Omega = \sin(\Theta)d\theta d\phi$. The original PYTHIA implementation is evidently distributed uniformly in θ . It was checked that all distributions are uniform in the azimuth angle ϕ .

From now on, the two coordinates p_T and η are used to analyze the kinematics as these are also the variables the cuts are performed on. Due to the relation $\eta = -\ln(\tan(\theta/2))$, the η -distributions will differ from the θ -distributions. The η -distributions were not normalized with the solid angle element. Therefore, the isotropic case in figure 5.1 shows an excess of emission for $|\eta| \rightarrow 0$ ($\theta \rightarrow \pi/2$), corresponding to the larger solid angle element in this area. In order to distinguish the η -distributions for different polarization cases, the ratios of rates in the polarized case and the isotropic case are shown. Higher relative fluctuations become prominent for $|\eta| > 1.5$. This is because of significantly lower statistics in these phase space regions due to the smaller solid angle element. The applied cuts at $\eta = \pm 0.8$ are shown as vertical dashed lines.

The measured acceptances α_η (only η -cut) are shown in tables 5.1 for the primary decay and 5.2 for the secondary decay. The obtained values for the relative acceptance deviate from the analytically expected values derived in chapter 3.3 within $-0.5\% < \Delta_{rel} < +4.2\%$. The obtained statistical errors are of the order of 10^{-4} and clearly underestimate the acceptance error (see section 5.5). The reason for these deviations has yet to be clarified. Nevertheless, these results are an important consistency check for the further proceedings.

Variable	Analytic	MC measurement	Relative deviation Δ_{rel}
primary decay $D^{*+} \xrightarrow{(1)} \pi^+ + D^0$			
α_η^0	0.649	0.663	+2.2%
α_η^t	0.836	0.850	+1.7%
α_η^l	0.274	0.292	+6.6%
$\alpha_\eta^t/\alpha_\eta^0$	1.288	1.281	-0.5%
$\alpha_\eta^l/\alpha_\eta^0$	0.424	0.441	+4.0%

Table 5.1: MC acceptance D^* of the primary decay for different polarization states $|\vec{p}(D^*)| \approx 0$ GeV, $\vec{p}(D^*) \parallel \vec{e}_z$ for 10^6 events.

Variable	Theory	MC measurement	relative deviation Δ_{rel}
secondary decay $D^0 \xrightarrow{(2)} \pi^+ + K^-$			
α_η^0	0.421	0.435	+3.3%
α_η^t	0.543	0.558	+2.8%
α_η^l	0.178	0.192	+7.9%
$\alpha_\eta^t/\alpha_\eta^0$	1.288	1.282	-0.5%
$\alpha_\eta^l/\alpha_\eta^0$	0.424	0.442	+4.2%

Table 5.2: MC acceptance D^* of the secondary decay for different polarization states $|\vec{p}(D^*)| \approx 0$ GeV, $\vec{p}(D^*) \parallel \vec{e}_z$ for 10^6 events.

In general, the central barrel detectors will not be able to detect particles in beam direction. Therefore, it is suitable to look at D^* particles with $\vec{p}(D^*) \parallel \vec{e}_x$, lying in the plane perpendicular to the beam axis. For a quasi-resting D^* , the spatial distributions of decay daughters when applying the Collins-Soper frame will be the same as for $\vec{p}(D^*) \parallel \vec{e}_z$ as they are independent of the direction of D^* momentum. Figure 5.2 shows the spatial distributions of decay daughters when applying the helicity frame, rotated by $\Delta\theta = \pi/2$ around the y -axis. Compared with figure 5.1, the η -distributions seem to switch places. Thus, longitudinally polarized D^* mesons decaying in the plane perpendicular to the beam axis will yield η -distributions of decay daughters in the helicity frame similar to those of transversely polarized mesons do in the Collins-Soper frame. We will see this “exchange of states” in the acceptance analysis.

As the detectors are also not able to detect quasi-resting D^* mesons due to the low momentum of the soft pion in the D^* rest frame, we will have to look at particles with $p_T > 0$ and consider the Lorentz transformation which distorts the distributions observed in the lab frame. This will influence the acceptance effect substantially, which is why we expect a strong p_T dependence.

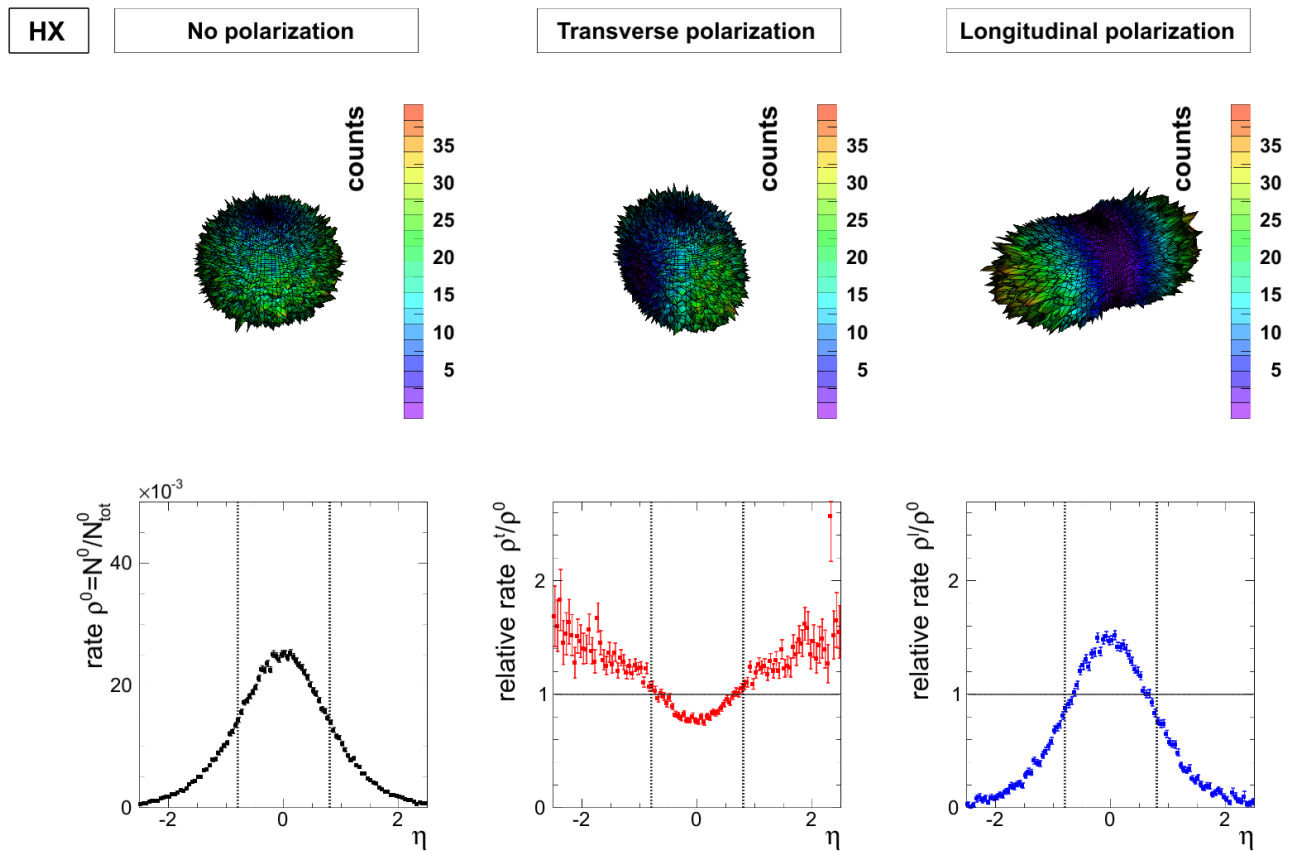


Figure 5.2: Spatial distribution of soft pion from D^* -decay for different polarization states with $|\vec{p}(D^*)| \approx 0$ GeV, $\vec{p}(D^*) \parallel \vec{e}_x$ for 10^5 events.

5.2 Acceptance effects due to η -cut

5.2.1 Effect of increasing $p_T(D^*)$, $y(D^*) = 0$

For increasing p_T , the daughter particles momentum vector components parallel to the D^* -momentum are enhanced due to the Lorentz boost along the D^* momentum direction. As discussed in chapter 3.1, the momentum of particles from the primary decay is then dominated in magnitude and direction by the momentum carried by the mother particle. For this reason, we expect the difference between the spatial distributions in the lab frame and therefore the relative acceptance effect between different polarization states to diminish for increasing p_T . Figure 5.3 shows the spatial distributions of the soft pion for D^* mesons with $\vec{p}(D^*) \parallel \vec{e}_x$ and $|\vec{p}(D^*)| = 0.5$ GeV. The three-dimensional representations of spatial distributions are evidently distorted in direction of the D^* momentum direction ($\eta = 0$). The η -distributions are also contracted towards $\eta = 0$. In the case of longitudinal polarization, the soft pions emitted in backward direction in the rest frame bring about a pair of bumps symmetric around $\eta = 0$ due to their boost in the direction of the D^* momentum. We will see that these bumps move towards $\eta = 0$ for even higher p_T and play an important role in understanding the acceptance effect.

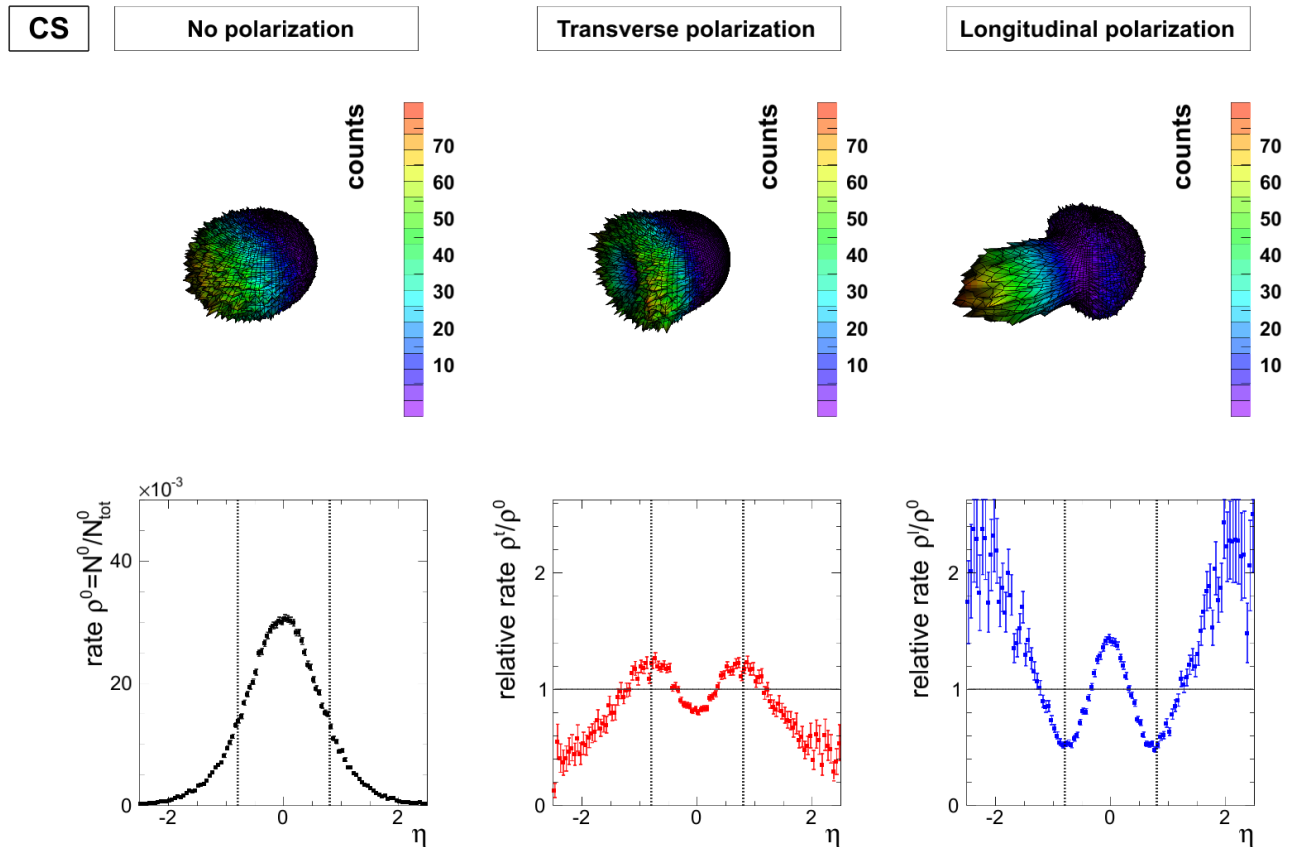


Figure 5.3: Spatial distribution of soft pion from D^* -decay for different polarization states in the helicity frame with $|\vec{p}(D^*)| = 0.5$ GeV, $\vec{p}(D^*) \parallel \vec{e}_x$ for 10^5 events.

The spatial distributions of the remaining particles are shown in figure 5.4. The η -distributions of the D^0 mesons show similar differences between polarized and isotropic cases as seen for the soft pion. As expected in the discussion of the decay kinematics in 3.1, the D^0 meson is strongly boosted in the direction of the D^* meson ($\eta = 0$) leading to a distribution peaked around $\eta = 0$, while the soft pion is emitted over a wide η -range. Therefore, the differences between the spatial distributions for polarized and unpolarized cases will not have a significant influence on the η -distributions of secondary pions π_2^+ and kaons stemming from D^0 decays. This is confirmed by the obtained relative distributions between polarized and unpolarized cases, which are unity within statistical errors except for minor fluctuations at high pseudorapidities. In consequence, only the soft pion will contribute to the acceptance effect due to the η -cut for increasing $p_T(D^*)$.

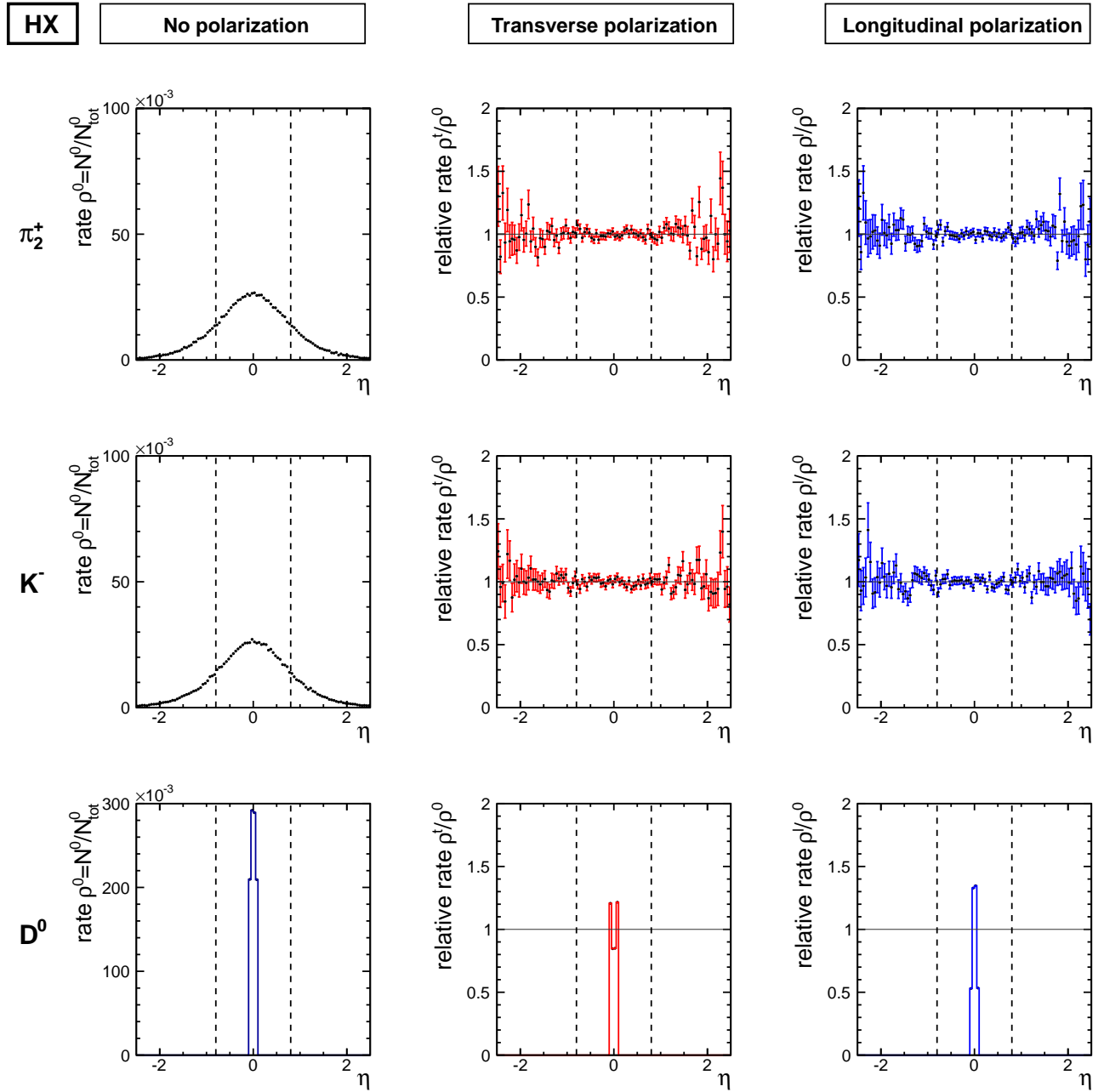


Figure 5.4: Spatial distribution of D^0 and decay daughters K^- , π_2^+ from D^* -decay for different polarization states in the helicity frame with $|\vec{p}(D^*)| = 0.5$ GeV, $\vec{p}(D^*) \parallel \vec{e}_x$ for 10^5 events.

After understanding in principle the effect of rotations and Lorentz transformations on spatial distributions, we will begin quantifying the acceptance effects for different $\vec{p}(D^*)$. Figure 5.5 shows the η -distributions of the soft pion for a D^* meson with $\vec{p}(D^*) \parallel \vec{e}_x$ and increasing p_T . For a transversely polarized, quasi resting D^* meson, we see an excess of soft pions outside and a deficiency inside the η -acceptance range of the detector compared to the isotropic case. The relative acceptance α^t/α^0 will then be smaller than 1. As discussed above, these structures will

be contracted toward $\eta = 0$ for higher p_T , leading to a deficiency at high pseudorapidity which counteracts the effect at zero p_T . Depending on the exact shape of the η -distribution, this can even lead to a relative acceptance slightly larger than 1.

For a longitudinally polarized, quasi resting D^* meson, the opposite is the case and we measure $\alpha^l/\alpha^0 > 1$. Increasing p_T results in two symmetrical bumps as described above, leading to an excess of particles at high pseudorapidity, which again counteracts the acceptance effect and can even lead to its inversion.

The distortion of distributions through Lorentz transformation with the associated compensational effect leads to a diminishing relative acceptance effect for increasing p_T . This happens at the latest when all soft pions are boosted in such a way that they are all within the acceptance range of the detector, which is the case for $p_T \approx 1$ GeV for D^* mesons in the plane perpendicular to the beam axis.

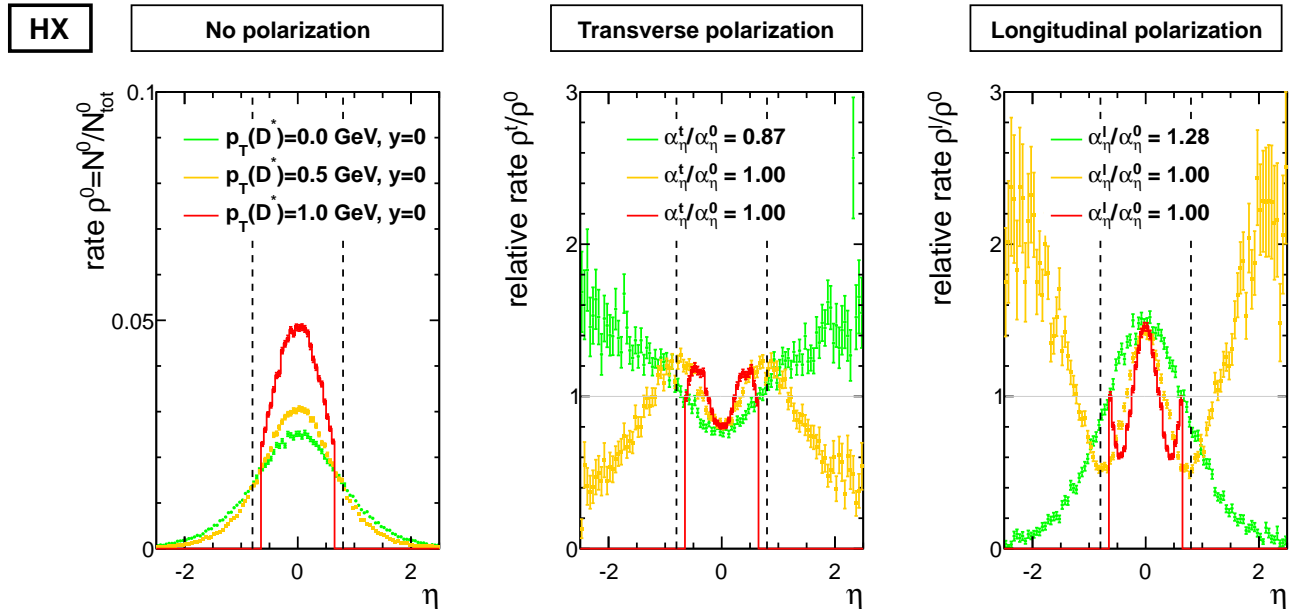


Figure 5.5: Spatial distribution of soft pion from D^* -decay for different polarization states and increasing momentum in the helicity frame with $|\vec{p}(D^*)| \in \{0.0, 0.5, 1.0\}$ GeV, $\vec{p}(D^*) \parallel \vec{e}_x$ for 10^6 events per p_T bin.

5.2.2 Effect of flat distribution in $|y(D^*)| < 0.5$

In general, D^* mesons at non-zero rapidity y with a momentum vector outside of the plane perpendicular to the beam axis are measured. This has been taken into account in the simulation by randomizing $y(D^*)$ as described in chapter 4.2. The effect of this rapidity distribution on the spatial distributions is shown for $p_T(D^*) = 0.5$ GeV in figure 5.6. Apparently, it smears out the η -distributions. This has two effects:

- The specific structures of the distribution in the polarized case are widened toward the edges of the distribution and flattened in the mid-pseudorapidity region. This can lead to an inversion of the overall acceptance effect compared to particles decaying in the plane perpendicular to the beam axis.
- A much higher $p_T(D^*)$ is needed to boost the decay particles in such a way that they are completely within the acceptance range. The effect is thereby extended to higher p_T .

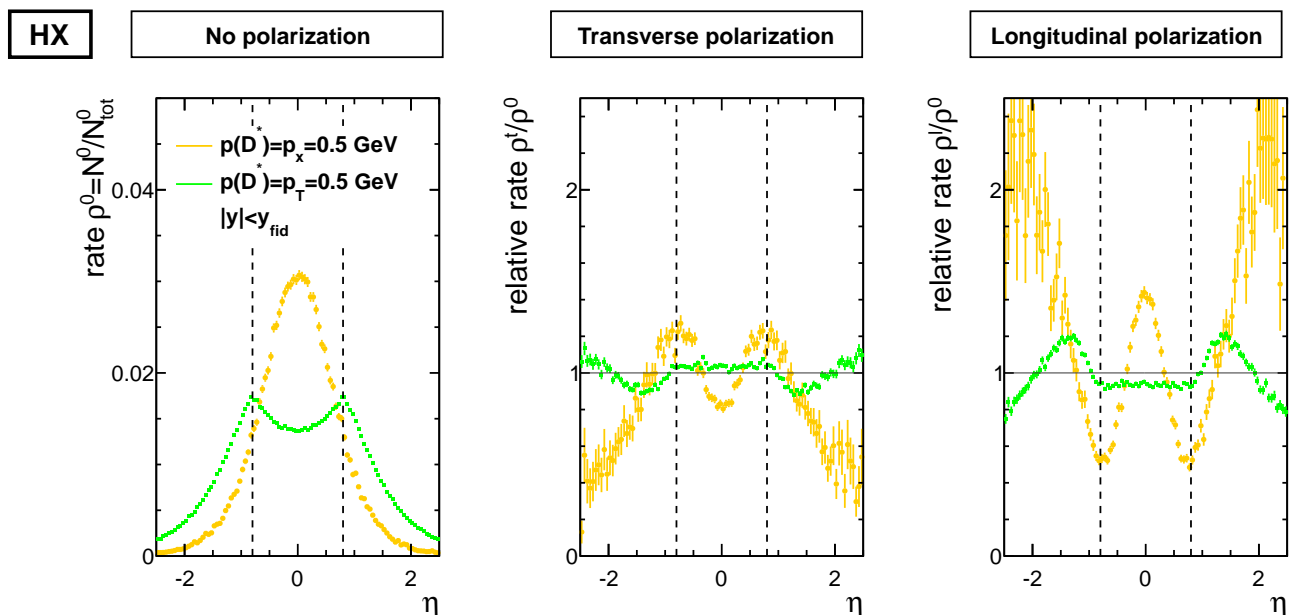


Figure 5.6: Spatial distribution of soft pion from D^* -decay for different polarization states in the helicity frame with $p_T(D^*) = 1$ GeV. Comparison of $y(D^*) = 0$, $y(D^*) \in [-0.5, +0.5]$ for 10^6 events.

The change of distributions for a D^* with flat rapidity distribution in $|y| < 0.5$ is shown for increasing p_T in 5.7. As in the case of D^* particles decaying in the plane perpendicular to the beam axis, the Lorentz boost leads to secondary structures at the edges of the spectra. These play an important role for the acceptance effect. Figure 5.8 shows the corresponding distributions in the Collins-Soper frame. Apparently, the effects of Lorentz transformation and the flat rapidity distribution of D^* mesons lead to nearly matching distributions for helicity and

Collins-Soper frames. Thus, our observation “state mirroring” for quasi-resting D^* particles and particles decaying in the plane perpendicular to the beam axis is no longer seen. However, the remaining structures are more prominent for the Collins-Soper frame, which is why we expect a larger acceptance effect in this case.

For $p_T \gtrsim 2$ GeV, only D^* particles decaying close to the acceptance boundary ($y(D^*) \approx 0.5$) contribute to the acceptance effect for the case that the decay products have a higher probability of being emitted outside (transverse for helicity frame) or inside (longitudinal for helicity frame) the acceptance range. The decay products of all D^* particles with lower rapidity will be boosted in such a way that they are within the η acceptance range of the detector regardless of their spatial distribution in the D^* rest frame. This edge effect, which is again inverted between the two reference frames, leads to an acceptance effect of $< 1\%$ and is therefore negligible compared to other errors of the cross section measurement. It will however contribute to the combined acceptance α calculated in chapter 5.4 with diminishing magnitude for rising p_t .

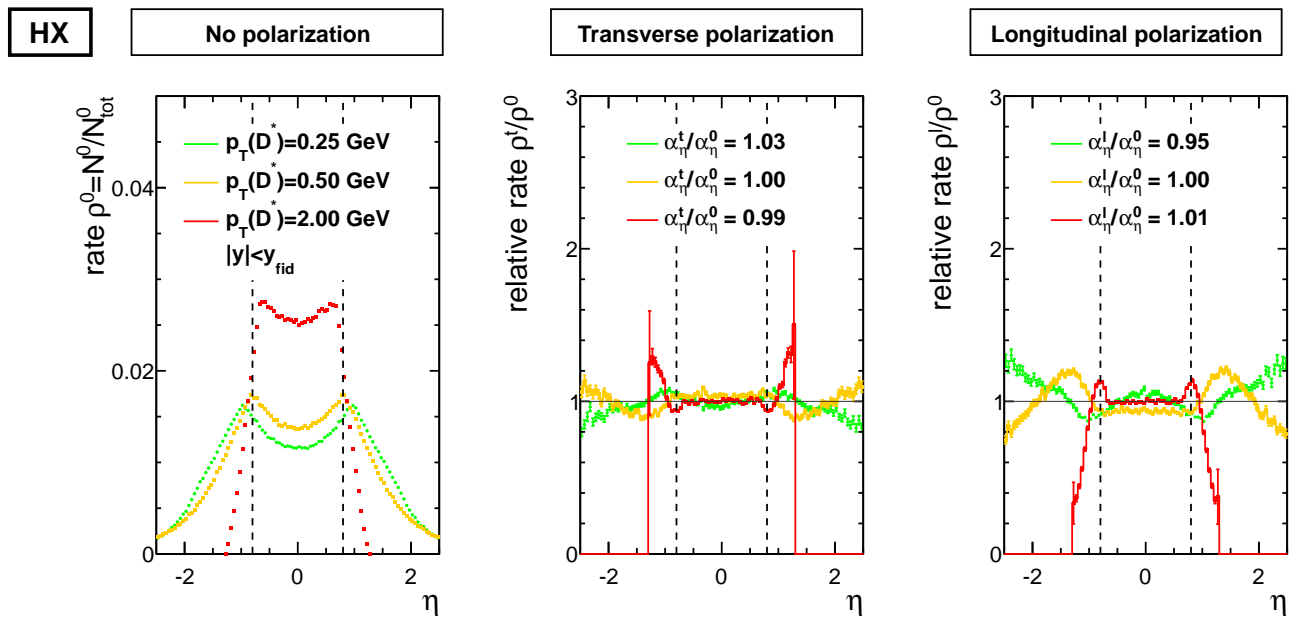


Figure 5.7: Spatial distribution of soft pion from D^* -decay for different polarization states in the helicity frame with $p_T(D^*) \in \{0.5, 1.0, 2.0\}$ GeV, $y(D^*) \in [-0.5, +0.5]$ for 10^6 events per p_T -bin.

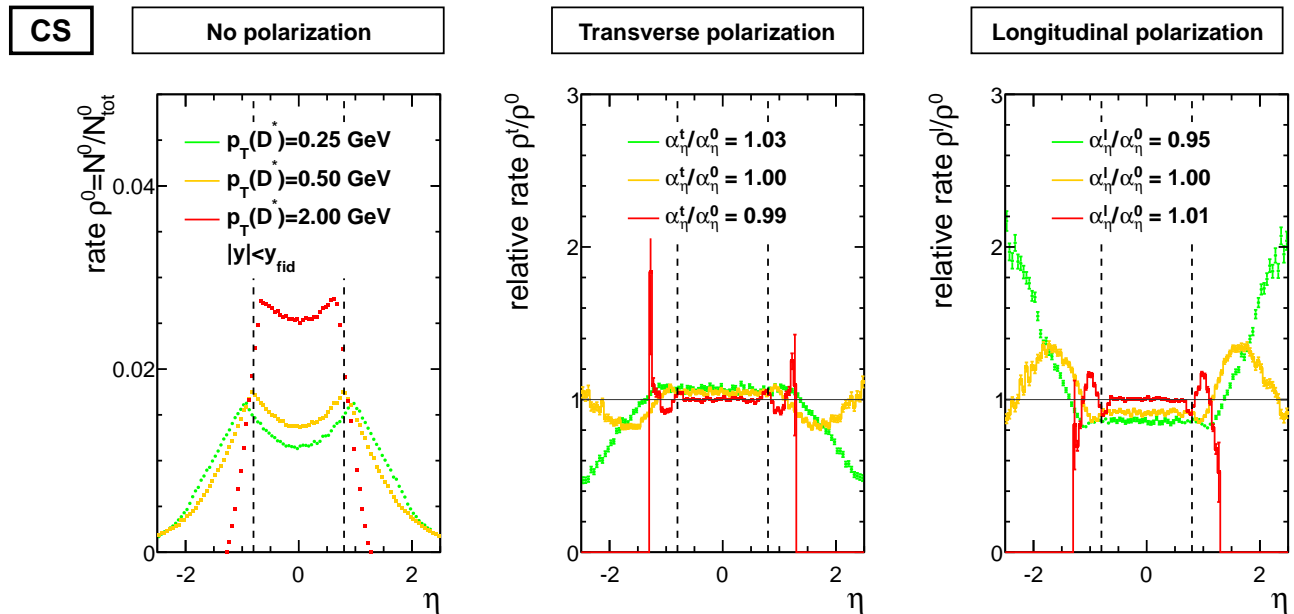


Figure 5.8: Spatial distribution of soft pion from D^* -decay for different polarization states in the Collins-Soper frame with $p_T(D^*) \in \{0.5, 1.0, 2.0\}$ GeV, $y(D^*) \in (-0.5, +0.5)$ for 10^6 events per p_T bin.

5.2.3 Acceptance effect for increasing p_T

Figure 5.9 shows the resulting acceptance effects in the helicity frame for $p_T(D^*) < 2$ GeV. As expected, the magnitude of the relative acceptance effect is the greatest for D^* mesons with very low p_T and quickly diminishes. We will consider a relative acceptance to “diminish” when it differs from unity within 1%. This is a reasonable definition, as the statistical and systematic errors of the cross section measurement outweigh an acceptance effect of this magnitude. With this definition, the acceptance effect diminishes for $p_T > 0.7$ GeV. The “oscillation” below 1 GeV originates from the secondary structures in the η -spectrum emerging for higher p_T (see 5.2.1), leading to a compensation of the acceptance effect.

As explained in chapter 5.2.2, the soft pion η -distributions are similar for helicity and Collins-Soper frame, leading to an enhanced acceptance for transverse polarization and reduced acceptance for longitudinal polarization compared to the isotropic case at low p_T . Figure 5.10 shows the acceptance effect in the Collins-Soper frame. Due to the specific structures in the η -distributions, the magnitude of the effect is larger for this frame, showing no “oscillation” as in the helicity frame. The effect diminishes at higher transverse momentum above 1.1 GeV. In the D^* analyses performed within the ALICE Collaboration, no cross section measurements were made for $p_T < 1$ GeV. The obtained acceptance effect due to η -cuts will therefore have no significant influence on $\alpha \times \epsilon$ and the cross section. However, the next chapter will show that there are more significant polarization effects that have to be taken into account.

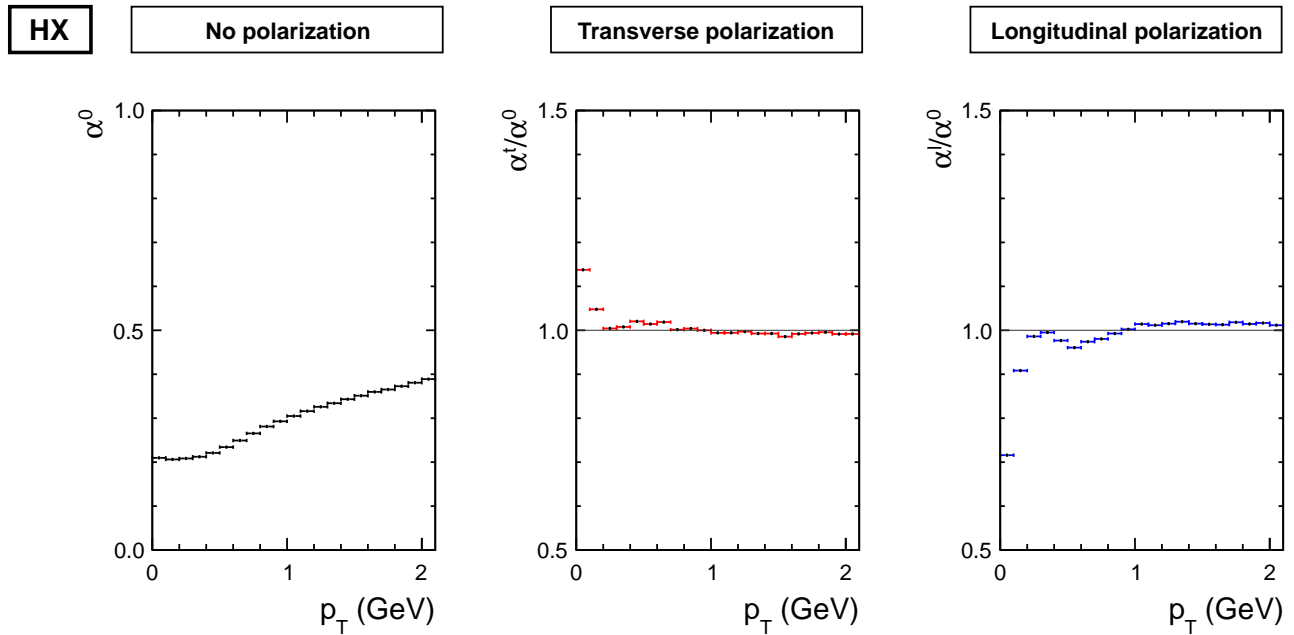


Figure 5.9: Acceptance α_η of D^* meson due to η -cut in the helicity frame for different polarization states and 10^7 events per p_t bin. $p_T(D^*) \in [0, 2]$ GeV, all values α_η above this range are within $[0.99, 1.01]$. $\Delta p_T = 0.1$ GeV.

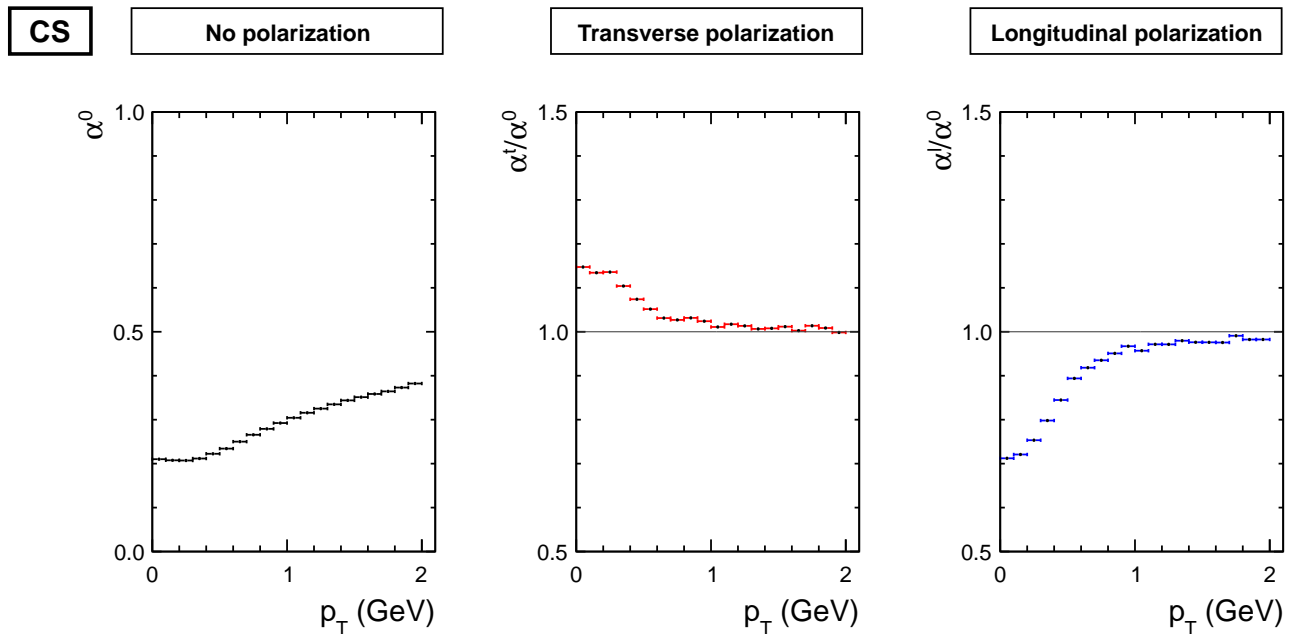


Figure 5.10: Acceptance α_η of D^* meson due to η -cut in the Collins-Soper frame for different polarization states and 10^6 events per p_t bin. $p_T(D^*) \in [0, 2]$ GeV, all values α_η above this range are within $[0.99, 1.01]$. $\Delta p_T = 0.1$ GeV.

5.3 Acceptance effects due to p_T -cut

We will now study the acceptance effect of the p_T -cuts on decay daughters due to different polarization states. In all analyses of this chapter, no η -cuts have been applied.

Only the p_T -cuts used in the cross section analysis of D^* in pp collisions will be studied step-by-step. The (higher p_T) cuts in the Pb-Pb analyses have analogous effects that are shown in chapter 5.3.3.

5.3.1 Shape of p_T -spectra of decay products

The obtained p_T -spectra of all decay daughters for D^* mesons with $p_T = 0.5$ GeV and uniform rapidity distribution in $|y| < 0.5$ are shown in figure 5.11 for the helicity frame. The cuts at $p_T = 80$ MeV for soft pions and $p_T = 400$ MeV for secondary pion and kaon are indicated by dashed vertical lines.

The p_T -spectrum of D^0 mesons is peaked close to the D^* momentum of $p_T = 0.5$ GeV, while the soft pion (π_1^+) p_T -spectrum lies entirely below 100 MeV. This is consistent with the consideration of kinematics in chapter 3.1 and the discussion of figure 5.4, where the D^0 meson receives most of the D^* momentum. Apparently, all soft pions have a transverse momentum below the cut. The acceptance will therefore vanish for $p_T(D^*) \lesssim 0.5$. This is in agreement with the threshold calculated in section 3.1.

Both the soft pion and the D^0 meson show significantly different p_T distributions for polarized decays than in the isotropic case. This can easily be understood when considering that the probability of emission along the D^* momentum axis is higher for longitudinal polarization in the helicity frame. These particles carry maximum momentum for emission parallel to the direction of the decaying particle and minimum momentum for emission antiparallel to the direction of the decaying particle. This leads to an excess of particles at the boundaries of the spectrum. For transverse polarization, the probability of emission perpendicular to the direction of the decaying particle is enhanced, leading to an excess of particles toward the middle of the continuum.

The secondary pion and kaon are distributed isotropically in the D^0 rest frame independent of the D^* polarization. Any difference between the p_T -spectra for polarized and non-polarized cases can therefore only originate from the initial p_T -distribution of the D^0 mother particle. The obtained spectra are wide compared to spectra from the primary decay. This was to be expected due to the much higher initial momentum in the D^0 rest frame (higher mass difference). The ratio of polarized and isotropic case is unity over most of this range in good approximation.

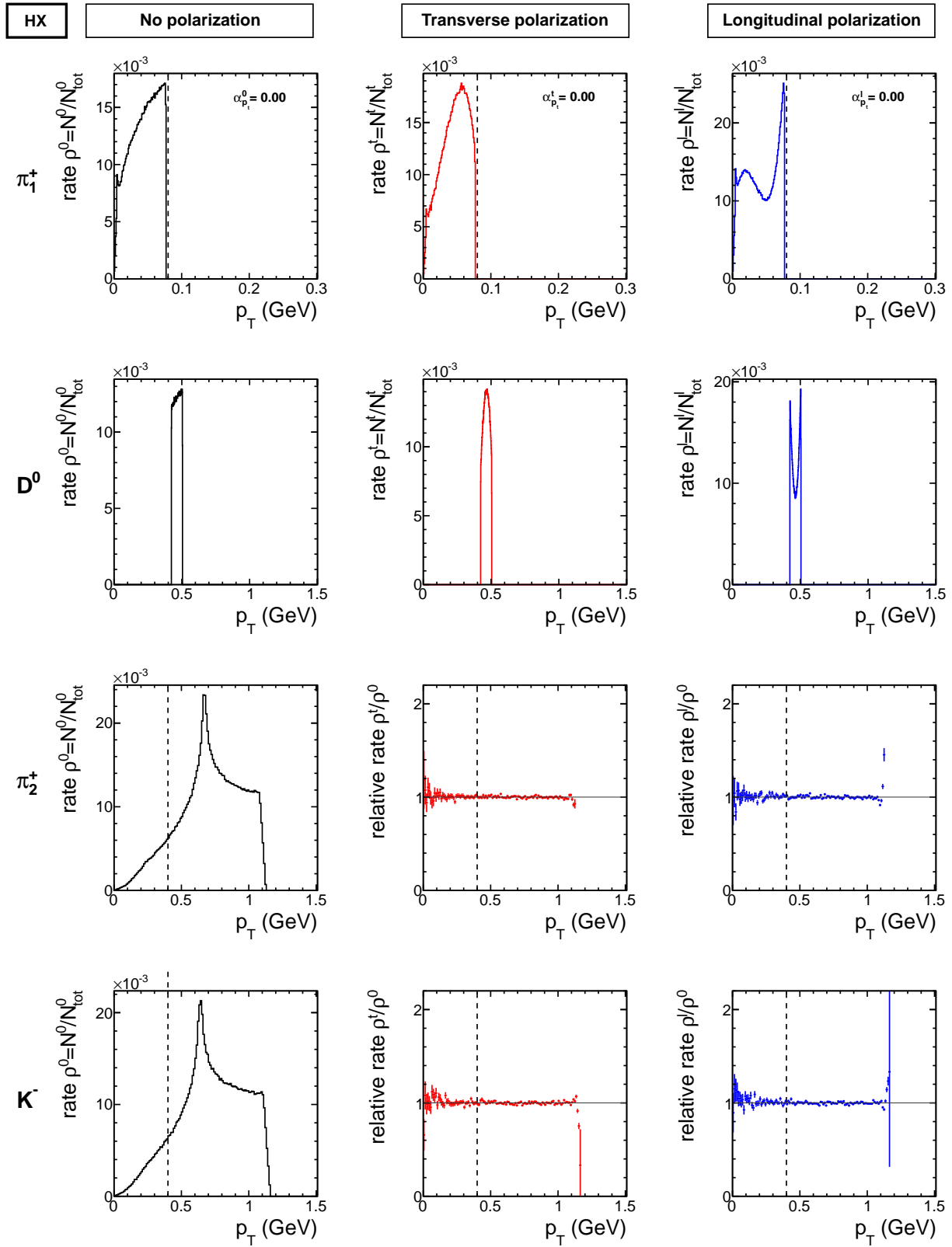


Figure 5.11: p_T -spectra of D^* decay products (soft pion π_1^+ , D^0 from primary decay and K^- , π_2^+ from secondary decay) in lab frame with polarization in the helicity frame and $p_T(D^*) = 0.5$ GeV, $y(D^*) \in [-0.5, +0.5]$ for 10^6 events.

The D^0 particles from the upper boundary of the D^0 p_T -spectrum will lead to a secondary pion and kaon p_T -spectrum shifted right compared to D^0 particles decaying on the lower boundary of the D^0 p_T -spectrum. In case of longitudinal polarization with an excess of particles in these areas of the spectrum, this can lead to an excess of particles at the boundaries of the secondary pion/kaon spectra. This can barely be seen when looking at the relative rates. The opposite effect occurs for transverse polarization, leading to slightly lower relative rates at the spectrum boundaries. As the secondary spectra are much wider than the primary spectra, this edge effect will not contribute considerably to the acceptance effect.

This becomes even clearer when we calculate the *particle specific* acceptance from these spectra:

$$\alpha_{p_T} = \frac{\int_{p_{T,min}}^{p_{T,max}} \rho(p_T) dp_T}{\int_0^{p_{T,max}} \rho(p_T) dp_T} \quad (21)$$

which is graphically just the fraction of the area below the spectrum above the p_T -cut (= number of particles in cuts) and the total area below the spectrum (= number of particles produced). An edge effect will have a diminishing influence on the relative acceptance due to the integration over the whole spectrum.

While secondary pions and kaons contribute to the *absolute* acceptance due to their continuous spectra below the p_T -cut for low $p_T(D^*)$, their contribution cancels out when calculating the *relative* acceptance between the different cases.

This leads to the conclusion that (again) only the soft pions show kinematics that significantly differ between decays of polarized and unpolarized D^* mesons.

5.3.2 Transverse momentum spectra of soft pion for increasing $p_T(D^*)$

For increasing D^* transverse momentum, the lower and upper boundaries of the soft pion spectra will be shifted to higher p_T with particles passing the p_T -cut. The soft pion p_T -spectra for increasing $p_T(D^*)$ are shown in figure 5.12 for the helicity frame.

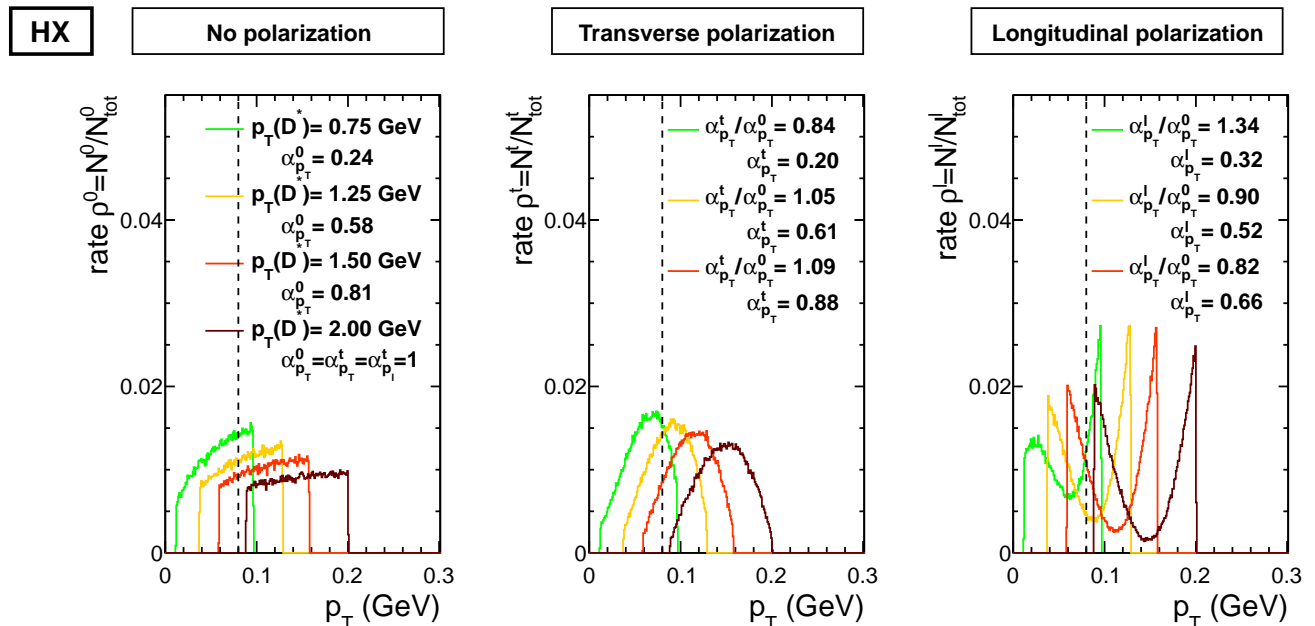


Figure 5.12: p_T -spectra of soft pion in lab frame with polarization in the helicity frame and $p_T(D^*) \in \{0.75, 1.25, 1.5, 2.0\}$ GeV, $y(D^*) \in [-0.5, +0.5]$ for 10^5 events per p_T bin. The soft pion acceptance is calculated from the spectra for each case with equation 21.

As discussed in the previous chapter, the acceptance of the soft pion for a certain $p_T(D^*)$ is given by the ratio of the spectrum area above the p_T -cut and the total area beneath the spectrum. For D^* decays just above the kinematic threshold at $p_T = 0.75$ GeV, the evident excess at the upper boundary of the spectrum for longitudinal polarization leads to a significantly higher soft pion acceptance than in the isotropic case. Analogously, the slope in the spectrum for transverse polarization leads to a lower acceptance than in the steeply rising, unpolarized case.

The effect decreases for increasing p_T . We observe that there is a specific $p_T(D^*)$ for which the fraction of area above the cut is the same for polarized and unpolarized case, leading to a relative acceptance $\alpha_{p_T}^{t,l} = 1$ at $p_T(D^*) \approx 1$ GeV. This value of p_T will be called the “crossing point” p_T^1 .

A further increase of p_T results in the inverse effect on α_{p_T} . This can be seen in the spectra for $p_T(D^*) = 1.5$ GeV. Due to the excess of particles at the lower boundary of the spectrum for the longitudinally polarized case, a lower fraction of particles will be above the p_T -cut than in the isotropic case. The opposite effect is observed for transverse polarization.

At $p_T(D^*) \approx 2$ GeV, all soft pions exceed the cut and the relative acceptance effect due to the different shapes of their p_T -spectra vanishes abruptly. As discussed above, the relative acceptance effect will be determined by the soft pion. We therefore expect the D^* acceptance to show a similar behavior.

Figure 5.13 shows the soft pion spectra for increasing $p_T(D^*)$ in the Collins-Soper frame. As in case of the η -distributions, the soft pion p_T -spectra of transversely and longitudinally polarized D^* mesons seem to “exchange states” compared to the helicity frame.

Due to the less prominent peaks at the boundaries of the p_T -spectrum when applying the Collins-Soper frame, the relative acceptance effects due to the soft pion p_T -cut are expected to be smaller in magnitude than those seen when applying the helicity frame.

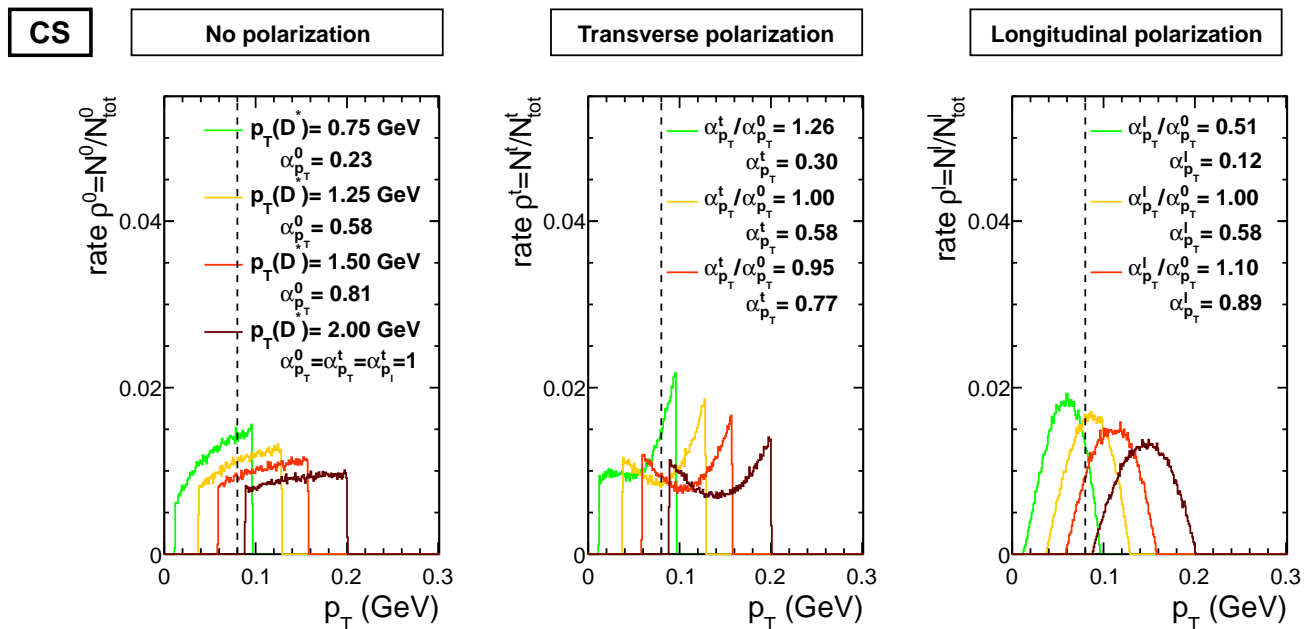


Figure 5.13: p_T -spectra of soft pion in lab frame with polarization in the Collins-Soper frame and $p_T(D^*) \in \{0.5, 1.25, 1.5, 2.0\}$ GeV, $y(D^*) \in [-0.5, +0.5]$ for 10^5 events per p_T bin. The soft pion acceptance is calculated from the spectra for each case with equation 21.

5.3.3 Acceptance effects

Figure 5.14 shows the resulting acceptance of the D^* meson with a p_T -cut of 80 MeV on the soft pion and 400 MeV on the daughters of the secondary decay. The oscillating structure reflects the transition of the soft pion p_T spectra over the p_T threshold as discussed in the last section. At $p_T^1 \approx 1$ GeV, the acceptances of isotropic and anisotropic cases coincide, leading to a relative acceptance $\alpha_{rel}^{t,l} = 1$. As expected, the relative acceptance effect is inverted for transverse polarization compared to longitudinal polarization. The magnitude is however different for the two cases. This will lead to an asymmetric uncertainty of the cross section measurement. Due to the “right tilt” of the spectra, the relative effect is greater for the upper boundary of the spectrum passing the cut (at lower $p_T(D^*)$) than for the lower boundary passing the cut (at higher $p_T(D^*)$). It diminishes abruptly at $p_T \approx 2$ GeV, where the soft pion spectra lie completely above the p_T -cut. As the measurement of D^* cross sections in pp collisions is done for $p_T \in [1, 24]$ GeV [7], the obtained acceptance effect due to p_T -cuts will have an impact. While intuitively expecting an acceptance effect in case of polarized D^* mesons due to the geometry of the central barrel detector (resulting in the η -cut), these unanticipated results show that in fact the p_T -cuts have a much larger influence.

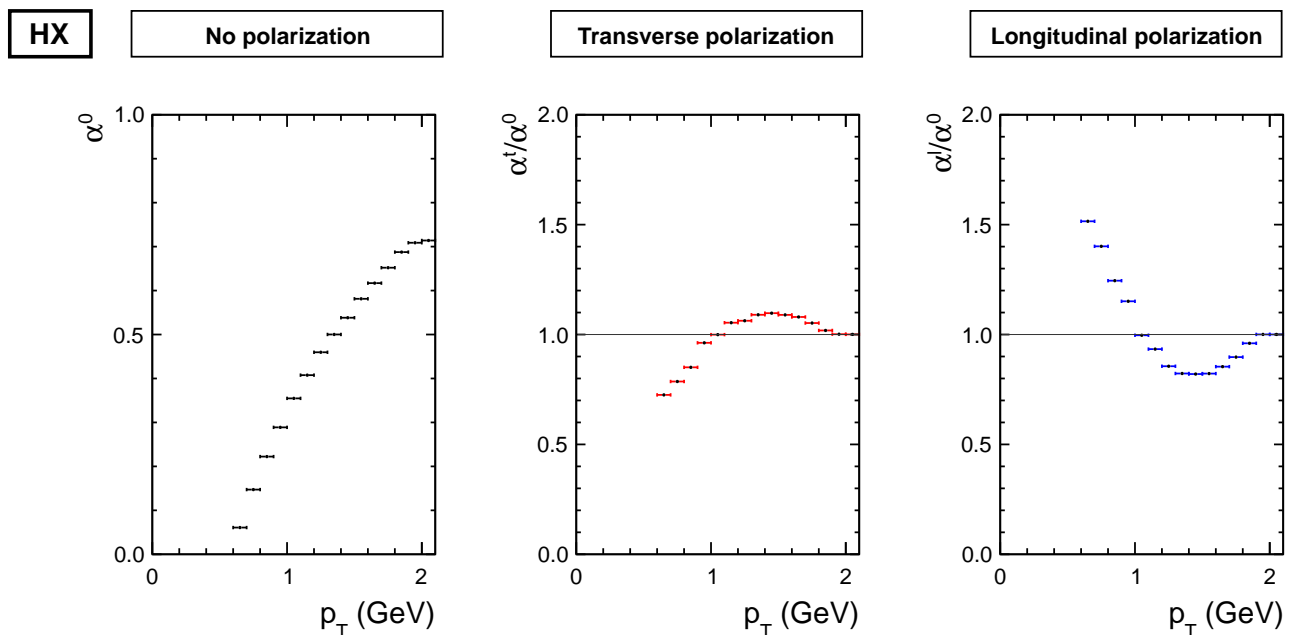


Figure 5.14: Acceptance α_{p_T} of D^* meson due to p_T -cut in the helicity frame for different polarization states and 10^6 events per p_t bin. $p_T(D^*) \in [0, 2]$ GeV, all values α_{p_T} above this range are within $[0.99, 1.01]$. $\Delta p_T = 0.1$ GeV.

Figure 5.15 shows the acceptance in the Collins-Soper frame. As expected, the acceptance effects of transverse and longitudinal polarization are inverted compared to the helicity frame (“exchange of states”).

Furthermore, the acceptances coincide for higher $p_T \approx 1.2$ GeV and the magnitude of the acceptance effect above this point is significantly smaller than in the helicity frame. This is due to the difference between the specific shapes of the p_T -spectra for the two frames.

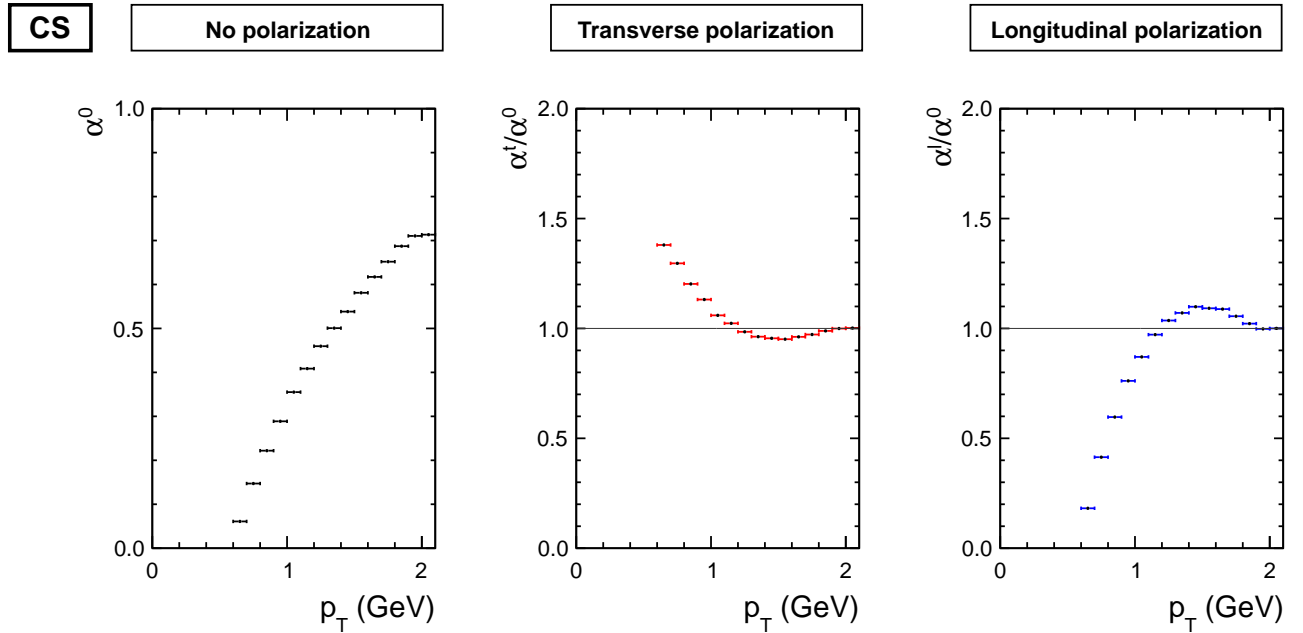


Figure 5.15: Acceptance α_{p_T} of D^* meson due to p_T -cut in the Collins-Soper frame for different polarization states and 10^6 events per p_t bin. $p_T(D^*) \in [0, 2]$ GeV, all values α_{p_T} above this range are within $[0.99, 1.01]$. $\Delta p_T = 0.1$ GeV.

After the discussion in chapter 5.3.2, we expect the acceptance curves to be shifted to higher p_T when increasing the p_T threshold of the soft pion. The acceptance effect for different thresholds is shown in figure 5.16 and shows exactly this behavior. The lower p_T threshold of D^* detection increases from around 0.5 GeV to 2 GeV when choosing a soft pion p_T -cut of 200 MeV instead of 80 MeV. The relative acceptance abruptly falls to unity when all soft pions are above the p_T cut. From now on, the value $\hat{p}_T(D^*)$ at which for all $p_T \geq \hat{p}_T$, $\alpha_{rel}^{t,l}(p_T)$ is within $[0.99, 1.01]$ for both longitudinal and transversal polarization will be called the “upper boundary” \hat{p}_T of the acceptance effect.

The upper boundaries $\hat{p}_T(\alpha_{p_T})$ are

- 1) $\hat{p}_T = 1.9$ GeV for $p_{T,min}(\pi_1^+) = 80$ MeV,
- 2) $\hat{p}_T = 2.2$ GeV for $p_{T,min}(\pi_1^+) = 100$ MeV,
- 3) $\hat{p}_T = 4.0$ GeV for $p_{T,min}(\pi_1^+) = 200$ MeV.

The choice of this p_T -cut thus has an important influence on the acceptance in the polarized as well as the unpolarized case.

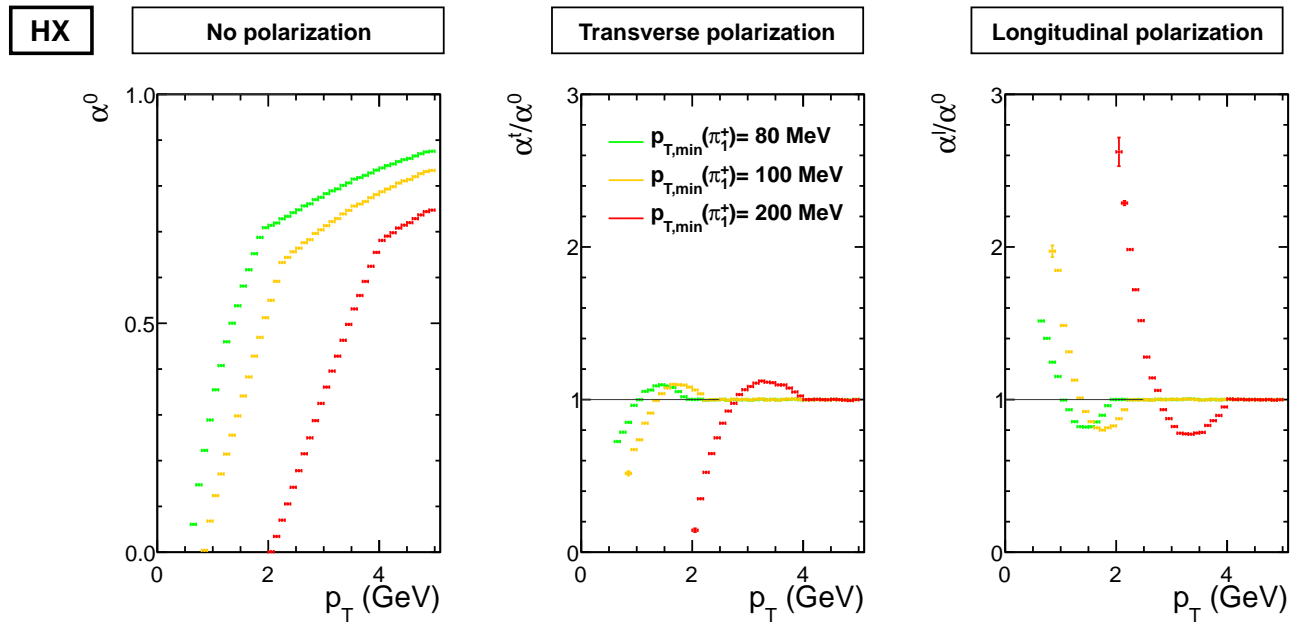


Figure 5.16: Acceptance α_{p_T} of D^* meson for different sets of p_T -cuts 3.3 in the helicity frame for different polarization states. $\Delta p_T = 0.1$ GeV. $p_T(D^*) \in [0, 5]$ GeV for 10^6 events per p_T -bin. All values α_{p_T} above this range are within $[0.99, 1.01]$.

5.4 Combined acceptance effects and implication on cross section measurements

The acceptance effects in the decays of polarized D^* mesons have been calculated and studied separately for η - and p_T -cuts on the decay daughters. In both cases, the effects are strongly p_T dependent. We have found that the combined acceptance effects will depend mainly on the p_T -cut on the soft pion while the η -cut has a negligible effect on our measurements. With this knowledge, the influence of the combined acceptance effect on the cross section measurement will be studied in this chapter.

The combined acceptance effect for the sets of cuts used in the cross section analyses is shown in figure 5.17 for the helicity frame. When comparing to figure 5.16 of the last chapter, where only p_T cuts were considered, one finds that while the η -cuts have a substantial effect on the magnitude and slope of the *absolute* acceptance, the *relative* acceptance is only marginally affected. The largest effect on the relative acceptance is below $p_T = 1$ GeV, as we expect from the discussion of α_η in chapter 5.2.3.

We can now compare the upper boundaries $\hat{p}_T(\alpha)$ to the p_T ranges of the D^* cross section measurements in table 5.3. Evidently, in measurements where the acceptance effect diminishes below the lower bound $p_{T,min}^\sigma$ of the range considered for the measurement, polarization will have no significant effect on the obtained cross section. Due to the relatively high $p_{T,min}^\sigma$ in the analyses of central Pb-Pb collisions (2,4 in table 5.3), polarization has no effect on these measurement for the chosen p_T -cuts on the soft pion.

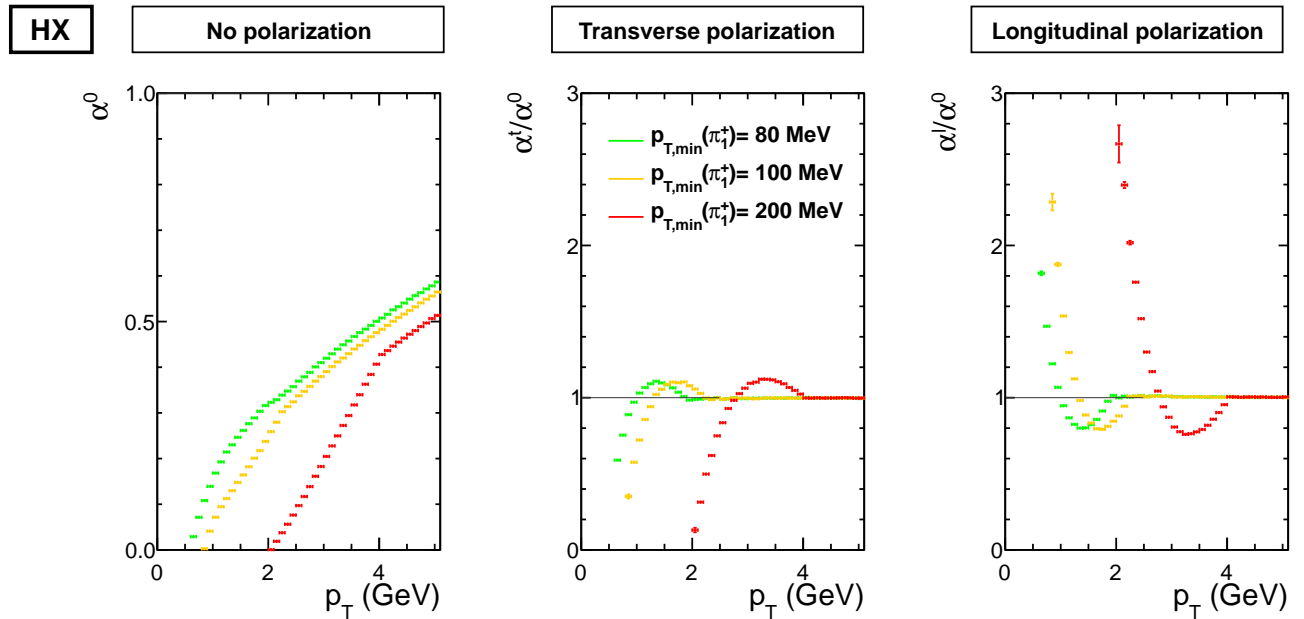


Figure 5.17: Acceptance α of D^* meson for different sets of p_T -cuts 3.3 in the helicity frame for different polarization states. $\Delta p_T = 0.1$ GeV. $p_T(D^*) \in [0, 5]$ GeV for 10^6 events per p_T -bin. All values α_{p_T} above this range are within $[0.99, 1.01]$.

#	Collision	p_T range (GeV)	$p_{T,min}(\pi_1^+)$ (GeV)	$\hat{p}_T(\alpha)$ (HX) (GeV)	$\hat{p}_T(\alpha)$ (CS) (GeV)
1	$pp, \sqrt{s} = 7$ TeV	[1.0,24.0]	0.08	2.1	1.9
2	Pb-Pb 2010, $\sqrt{s_{NN}} = 2.76$ TeV (centrality 0 – 20%)	[4.0,16.0]	0.2	4.0	4.0
3	Pb-Pb 2010, $\sqrt{s_{NN}} = 2.76$ TeV (centrality 40 – 80%)	[2.0,16.0]	0.1	2.4	2.2
4	Pb-Pb 2011, $\sqrt{s_{NN}} = 2.76$ TeV (centrality 0 – 7.5%)	[3.0,36.0]	0.1	2.4	2.2

Table 5.3: Transverse momentum measurement range and soft pion p_T cut for previous D^* cross section measurements [7, 11, 12] compared to the upper boundary \hat{p}_T of the acceptance effect. The upper boundaries are derived in appendix B.

For the analyses of peripheral Pb-Pb collisions (3) and pp collisions (1), the acceptance effect diminishes above $p_{T,min}^\sigma$ and we expect an effect on the cross section measurements.

The cross sections are measured in p_T -bins with width $\Delta p_T = 1$ GeV for low p_T up to $\Delta p_T = 8$ GeV for high p_T due to lower statistics in this region of phase space. The acceptance effects of polarization are calculated for $p_T \in [0, 30]$ GeV in steps of $\Delta p_T = 0.1$ GeV, requiring a rebinning of the calculated acceptance to the bin widths and limits of the cross section measurement. As the cross section is strongly dependent on p_T , a simple unweighted average corresponding to a flat distribution in p_T is inaccurate. Therefore, a weighted average is calculated for each bin by weighting with a normalized cross section spectrum based on a FONLL²-calculation [17, 18] with granularity $\Delta p_T = 0.1$ GeV. It has been shown that previous D^* cross section measurements in pp collisions agree with these calculations within errors [7]. The FONLL-spectrum underlies systematic uncertainties due to certain QCD parameters. The central values of the calculation are used for averaging. The deviation for averages performed with the upper and lower uncertainty limits of the spectrum is expected to be small due to normalization. The weighted average is calculated by:

$$\bar{\alpha}_{rel}^{ab} = \sum_{i=a}^b \alpha_{rel}^i \cdot \frac{d\sigma_{FONLL}^i}{dp_T} \cdot \left(\sum_k \frac{d\sigma_{FONLL}^k}{dp_T} \right)^{-1}$$

with a indicating the lower bin and b indicating the upper bin of the range averaged over. $\alpha_{rel}^i = \alpha^{t,l;i}/\alpha^{0;i}$ is the relative acceptance in bin i and $d\sigma_{FONLL}^i/dp_T$ the differential cross section of the FONLL-spectrum in this bin. The sum over k cumulates all entries of the histogram for normalization.

After rebinning the calculated acceptance effect for the p_T -cut of the soft pion at 100 MeV, the weighted average of $\bar{\alpha}_{rel}^t$ and $\bar{\alpha}_{rel}^l$ for all bins above $p_{T,min}^\sigma = 2$ GeV is within $[0.99, 1.01]$. The effect of polarization is thus also negligible for this cross section measurement with the chosen soft pion p_T cut. For the measurements in pp collisions, rebinning yields significant relative acceptances which will be studied further in the next section.

5.4.1 Polarization uncertainty of D^* cross section measurements in pp collisions

Figure 5.18 shows the calculated and rebinned relative acceptance for transverse and longitudinal polarization in the helicity frame for $p_T(D^*) \in [0.5, 24]$ GeV as well as the impact on the measured cross section. The average acceptance $\bar{\alpha}_{rel}^{t,l}$ significantly differs from unity asymmetrically by ${}_{-12.1}^{+5.9}\%$ in the lowest bin of the cross section measurement $p_T \in [1, 2]$ GeV. This leads to a corresponding (inverse) uncertainty of the cross section of ${}_{-5.6}^{+13.8}\%$ in this p_T region. The even higher effect below 1 GeV does not contribute to the measurement. This is generic for most of the Pb-Pb collision measurements where $p_{T,min}^\sigma$ lies just above the upper boundary $\hat{p}_T(\alpha)$ of the effect. One could consider this a lucky coincidence, as the polarization uncertainty for measurements at lower p_T would quickly be of the order of 30 – 40%.

In the cross section relevant bin $[1, 2]$ GeV, transverse polarization leads to a higher acceptance

²FONLL (First Order Next to Leading Log) is a framework for calculations in perturbative QCD.

and longitudinal polarization leads to a lower acceptance than in the isotropic case. This is inverse to the other bins and due to the oscillating structure of $\alpha_{rel}^{t,l}$. The integrated uncertainty of the cross section due to polarization in the helicity frame is ${}_{-2.5}^{+6.4}\%$ and thus significant compared to the other errors on the cross section measurement:

$$d\sigma^{D^*}/dy = 247 \pm 27(\text{stat.})_{-81}^{+36}(\text{syst.}) \pm 9(\text{lumi.}) \pm 4(\text{BR})_{-16}^{+57}(\text{extr.})_{-6}^{+16}(\text{pol. HX}) \mu\text{b} [7] \quad (22)$$

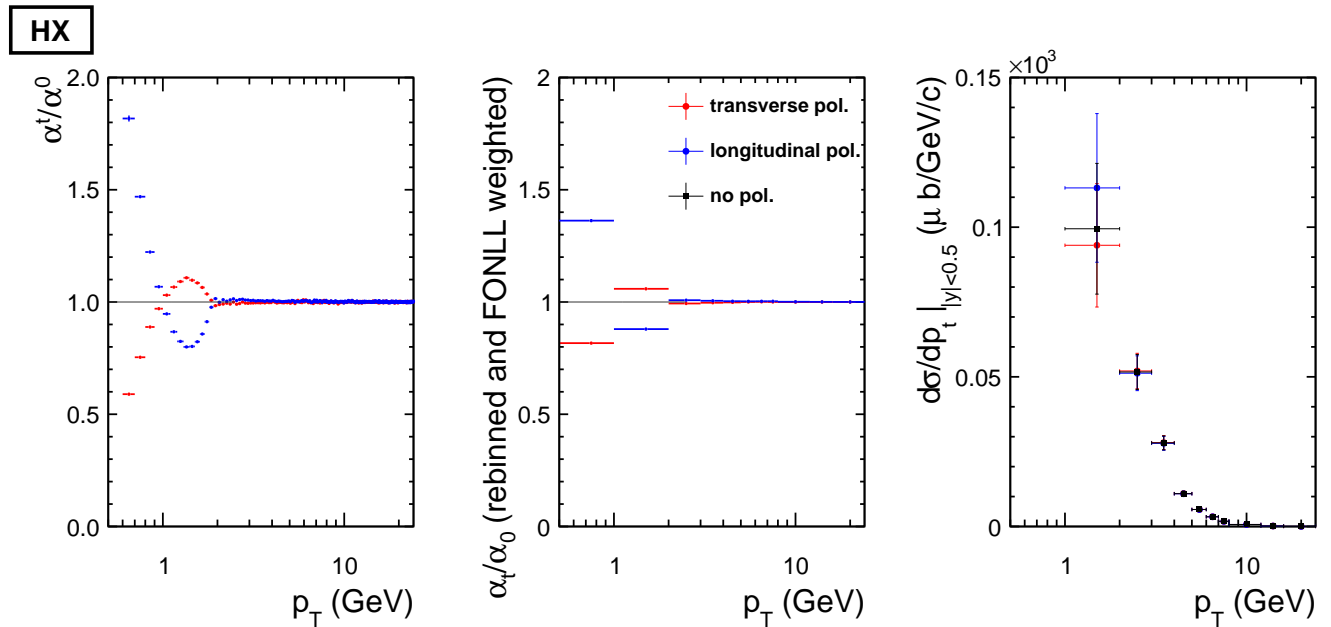


Figure 5.18: Cross section uncertainty due to polarization acceptance effects in the helicity frame for the D^* -analysis in pp collisions at $\sqrt{s} = 7$ TeV. MC Simulation with both η and p_T cuts on decay daughters. $p_T(D^*) \in [0.5, 24]$ GeV, $\Delta p_t = 0.1$ GeV for 10^6 events per p_T bin.

The corresponding analysis in the Collins-Soper frame is shown in figure 5.19. While the absolute magnitude of α_{rel}^l below 1 GeV is even larger than in the helicity frame, the acceptance effect in the relevant bin $p_T \in [1, 2]$ is barely significant with ${}_{-1.7}^{+1.0}\%$. On the one hand, this is due to the lower magnitude of the “oscillation” because of the less prominent boundary peaks in the soft pion p_T distribution for the Collins-Soper frame compared to the helicity frame. On the other hand, it is due to the crossing point p_T^1 being shifted to higher $p_T^1 \approx 1.2$ GeV. The acceptance effect in $p_T \in [1.0, 1.2]$ GeV and the opposite effect in $p_T \in [1.2, 2.0]$ GeV compensate each other. In the helicity frame, the crossing point lies at $p_T^1 \approx 1$ GeV and no compensation occurs within the bin. This binning effect leads to a negligible uncertainty of the integrated cross section due to polarization of ${}_{-0.6}^{+1.3}\%$ in this case. As we do not know the polarization state in neither reference frame, we have to assume the maximum uncertainty in the helicity frame calculated above.

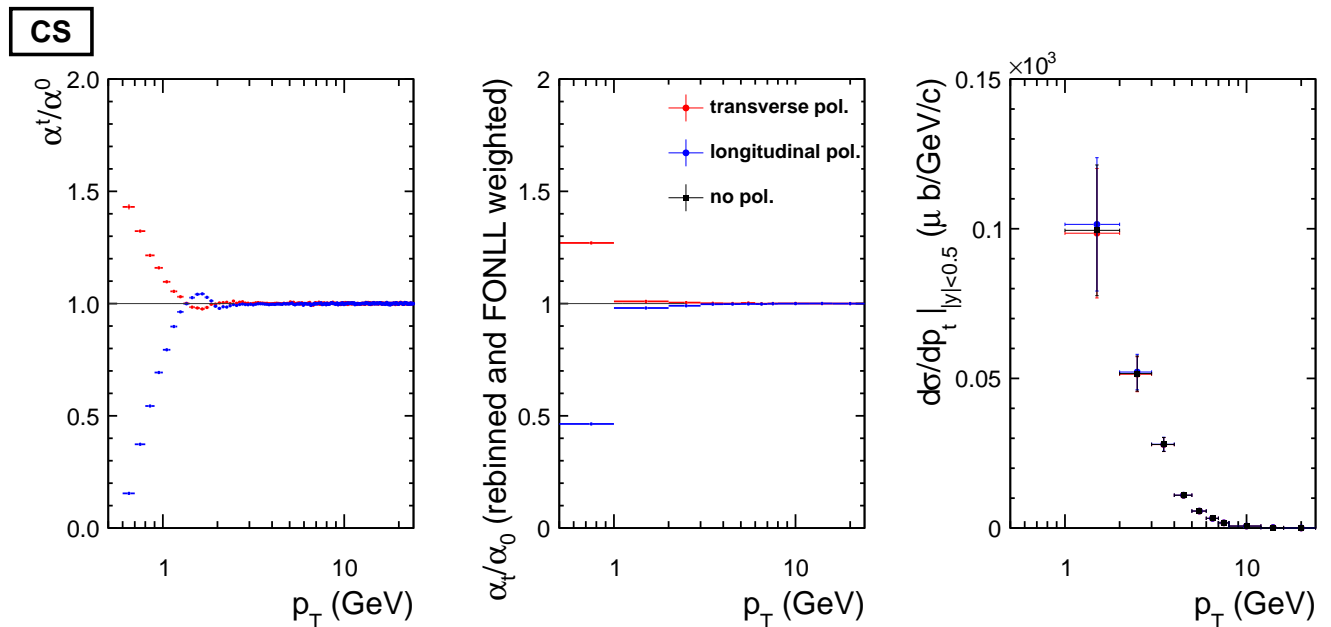


Figure 5.19: Cross section uncertainty due to polarization acceptance effects in the Collins-Soper frame for the D^* -analysis in pp collisions at $\sqrt{s} = 7$ TeV. MC Simulation with both η and p_T cuts on decay daughters. $p_T(D^*) \in [0.5, 24]$ GeV, $\Delta p_t = 0.1$ GeV for 10^6 events per p_T bin.

The obtained results imply that in future analyses, three parameters have to be very carefully handled when performing cross section analyses of the D^* meson:

- 1) **Soft pion p_T cut:** This parameter determines the p_T range of the acceptance effect due to polarization and the low- p_T threshold of D^* detection. It fixes crossing point p_T^1 and upper boundary \hat{p}_T of the effect.
- 2) **Lower bound $p_{T,min}^\sigma$ of cross section measurement:** When fixing this parameter, the upper boundary \hat{p}_T of the acceptance effect should be taken into account. For measurements below \hat{p}_T , the uncertainty due to polarization becomes significant and can even dominate over the other systematic and statistical errors of the cross section measurement.
- 3) **Binning:** All considered cross section measurements were binned in p_T with integer bin limits. A deviation from this convention when below \hat{p}_T can lead to compensational effects due to the oscillation of the acceptance curve, reducing the uncertainty due to polarization.

All these parameters evidently underlie further constraints. Nevertheless, polarization effects have to be taken into account for low p_T cross section measurements in order to limit the influence of polarization uncertainty. In future analyses, separate calculations of the acceptance for the different polarization cases and reference frames should be performed in order to be able to assess this influence when choosing the above parameters. This can easily be done by implementing the anisotropic spatial distributions of the decay daughters into the existing simulation frameworks as described in chapter 4.

5.5 Discussion of errors

As discussed in chapter 5.1, the high pseudorapidity regions of phase space of the daughter particles show relatively low statistics compared to the central region within $|\eta| < 1.5$. This is due to the smaller solid angle element $d\Omega/d\eta$ in this region and leads to higher statistical errors. These errors significantly impact the ratio of particles inside the η -cut to the ones outside the η -cut and thus the acceptance α_η . This is however not taken into account by the binomial error calculated for the acceptances, which *underestimates* the error.

This becomes particularly clear when calculating the acceptance curves $\alpha_\eta(p_T)$ with lower statistics of 10^5 events per p_T bin, where the obtained values fluctuated significantly around the values at higher statistics with vanishing errors. Therefore, a very high number of 10^7 events per p_T bin is simulated in order to calculate $\alpha_\eta(p_T)$ in the helicity frame, which is especially sensible to this effect due to the dependency of the spatial distributions on the D^* direction of motion. The p_T spectra are much less sensible to the number of events. Thus, only 10^5 to 10^6 events per p_T -bin suffice for results with negligible fluctuations.

In order to save computational power, only the analyses for which it was absolutely required to apply higher statistics in order to understand the underlying effects were computed with 10^6 or even 10^7 events per p_T bin. This leads to a heterogeneous number of events in some plots of this thesis which does not affect their physical statements. The possibility of obtaining virtually unlimited statistics when performing simulations should not lead to the urge to bring every last error to zero. With the given statistics, the relative acceptance $\alpha^{t,l}(p_T)/\alpha^0(p_T)$ fluctuates by about 0.5% around 1 at higher p_T . As an effect of this magnitude is negligible in view of the other statistical and systematic errors considered in cross section measurements, this level of accuracy suffices.

6 Conclusion

The effects of polarization in the decay $D^{*+} \rightarrow D^0(\pi^+K^-) + \pi^+$ and their influence on cross section measurements at ALICE were analyzed in this thesis.

It was shown that the decay products of polarized D^* mesons feature anisotropic spatial distributions. Due to the limited acceptance range $|\eta| < 0.8$ of the ALICE central barrel detectors, a difference between the acceptance for polarized and unpolarized D^* mesons was derived for D^* mesons decaying at rest, motivating further investigation.

In order to study this effect for general D^* momenta, a simulation macro was implemented by extending the PYTHIA decay routine with anisotropic distributions of decay products. The helicity and Collins-Soper frames were considered as two possible reference frames for polarization.

The expected acceptance effect due to the η -cut on decay daughters was confirmed for a resting D^* meson. The spatial distributions of the decay daughters in the lab frame are strongly modified for increasing D^* transverse momentum and the differences between polarized and unpolarized cases disappear. The acceptance effect due to the limited angular acceptance therefore diminishes below 1 GeV and is negligible for previous D^* cross section measurements, which do not cover this p_T region.

However, the analysis showed that the p_T -distributions of decay products are also influenced by polarization. The p_T -cut on the decay daughters leads to an additional acceptance effect which extends to much higher D^* transverse momenta up to 4 GeV, depending strongly on the choice of the soft pion p_T cut. Due to the specific decay kinematics, the low momentum soft pion dominates the acceptance effect for both η and p_T -cut.

The influence of this effect on the cross section mainly depends on two parameters: the lower p_T bound of the measurement $p_{T,min}^\sigma$ and the choice of the soft pion p_T -cut, which determines range and magnitude of the acceptance effect. In the previous analyses of the D^* cross section in Pb-Pb collisions, the lower bounds $p_{T,min}^\sigma$ lie just above the transverse momentum \hat{p}_T where the acceptance effect diminishes for the chosen soft pion p_T cuts. The cross section uncertainty due to polarization is therefore negligible for these measurements. In the analysis of pp collisions, the cross section value in [1, 2] GeV shows an uncertainty of ${}_{-5.6}^{+13.8}\%$ due to polarization, leading to an uncertainty of the integrated cross section of ${}_{-2.5}^{+6.4}\%$, which is significant compared to the remaining statistical and systematic uncertainties.

In future cross section measurements of D^* , these potential uncertainties have to be taken into account when choosing kinematic cuts and low p_T bins of the measurement. For soft pion p_T cuts at 80, 100 and 200 MeV, these considerations can be made with the help of the relative acceptance values calculated for different D^* transverse momenta in this project (tabulated in appendix B). For more general considerations, the derived angular distributions should be implemented in the $(\alpha \times \epsilon)$ calculations of the analysis by one of the methods described in chapter 4. The best way to eliminate this uncertainty would be a measurement of the D^* polarization as performed for the J/Ψ meson by the ALICE Collaboration [19].

References

- [1] F. Karsch, “Lattice simulations of the thermodynamics of strongly interacting elementary particles and the exploration of new phases of matter in relativistic heavy ion collisions,” *J.Phys.Conf.Ser.* **46** (2006) 122–131, arXiv:hep-lat/0608003 [hep-lat].
- [2] **ALICE** Collaboration, K. Aamodt *et al.*, “The ALICE experiment at the CERN LHC,” *JINST* **3** (2008) S08002.
- [3] Klein, Jochen, “Commissioning of and Preparations for Physics with the Transition Radiation Detector in A Large Ion Collider Experiment at CERN,”. Ph.D. thesis, University of Heidelberg.
- [4] A. Adil and I. Vitev, “Collisional dissociation of heavy mesons in dense qcd matter,” *Physics Letters B* **649** no. 2â3, (2007) 139 – 146.
<http://www.sciencedirect.com/science/article/pii/S0370269307004248>.
- [5] R. Sharma, I. Vitev, and B.-W. Zhang, “Light-cone wave function approach to open heavy flavor dynamics in QCD matter,” *Phys.Rev.* **C80** (2009) 054902, arXiv:0904.0032 [hep-ph].
- [6] J. Beringer *et al.* *Phys.Rev.* **D86** (2012) 010001. <http://pdg.lbl.gov/>. (Particle Data Group).
- [7] **ALICE** Collaboration, B. Abelev *et al.*, “Measurement of charm production at central rapidity in proton-proton collisions at $\sqrt{s} = 7$ TeV,” *JHEP* **1201** (2012) 128, arXiv:1111.1553 [hep-ex].
- [8] P. Faccioli, C. Lourenco, J. Seixas, and H. K. Wohri, “Towards the experimental clarification of quarkonium polarization,” *Eur.Phys.J.* **C69** (2010) 657–673, arXiv:1006.2738 [hep-ph].
- [9] J. C. Collins and D. E. Soper, “Angular Distribution of Dileptons in High-Energy Hadron Collisions,” *Phys.Rev.* **D16** (1977) 2219.
- [10] Private communication with Jochen Klein at Physikalisches Institut of the University of Heidelberg.
- [11] **ALICE** Collaboration, B. Abelev *et al.*, “Suppression of high transverse momentum D mesons in central Pb-Pb collisions at $\sqrt{s_{NN}} = 2.76$ TeV,” arXiv:1203.2160 [nucl-ex].
- [12] **ALICE** Collaboration, . Preliminary analysis of Pb-Pb collisions at $\sqrt{s_{NN}} = 2.76$ TeV in 2011 data. In process of publication.
- [13] M. Paterno, “Calculating efficiencies and their uncertainties,”
<http://home.fnal.gov/~paterno/images/effic.pdf>. FERMILAB-TM-2286-CD.

- [14] T. Sjöstrand, S. Mrenna, and P. Z. Skands, “PYTHIA 6.4 Physics and Manual,” *JHEP* **0605** (2006) 026, [arXiv:hep-ph/0603175](#) [hep-ph].
- [15] **ALICE** Collaboration, B. Abelev *et al.*, “Measurement of prompt and non-prompt J/ψ production cross sections at mid-rapidity in pp collisions at $\sqrt{s} = 7$ TeV,” [arXiv:1205.5880](#) [hep-ex].
- [16] Sjöstrand, Torbjörn and Mrenna, Stephen and Skands, Peter, “A Brief Introduction to PYTHIA 8.1,” <http://arxiv.org/abs/0710.3820>.
- [17] M. Cacciari, S. Frixione, N. Houdeau, M. Mangano, P. Nason, and G. Ridolfi, “Theoretical predictions for charm and bottom production at the LHC,” *Arxiv preprint arXiv:1205.6344* (2012) .
- [18] M. Cacciari, M. Greco, and P. Nason, “The p_t spectrum in heavy-flavour hadro-production,” *Journal of High Energy Physics* **1998** (1998) 007.
- [19] **ALICE Collaboration** Collaboration, B. Abelev *et al.*, “ J/ψ polarization in pp collisions at $\sqrt{s}=7$ TeV,” *Phys.Rev.Lett.* **108** (2012) 082001, [arXiv:1111.1630](#) [hep-ex].
- [20] Private communication with Robert Grajcarek at Physikalisches Institut of the University of Heidelberg.
- [21] R. Grajcarek. Ph.D. thesis, University of Heidelberg, in preparation.

A Figures of polarization effects in Collins-Soper frame

In this appendix, all the figures shown only for the helicity frame in section 5 are listed here for the Collins-Soper frame.

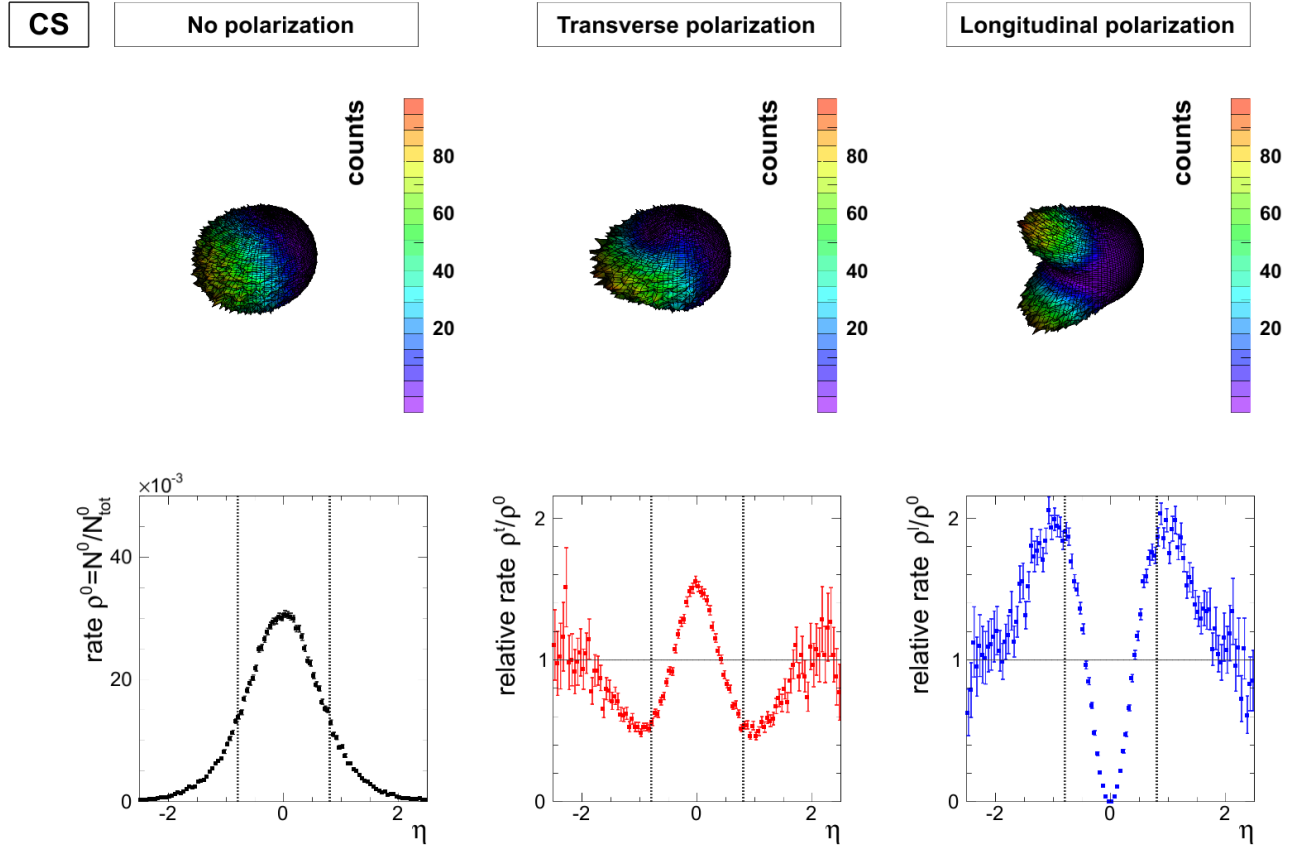


Figure A.1: Spatial distribution of soft pion from D^* -decay for different polarization states in the Collins-Soper frame with $|\vec{p}(D^*)| = 0.5$ GeV, $\vec{p}(D^*) \parallel \vec{e}_x$ for 10^5 events.

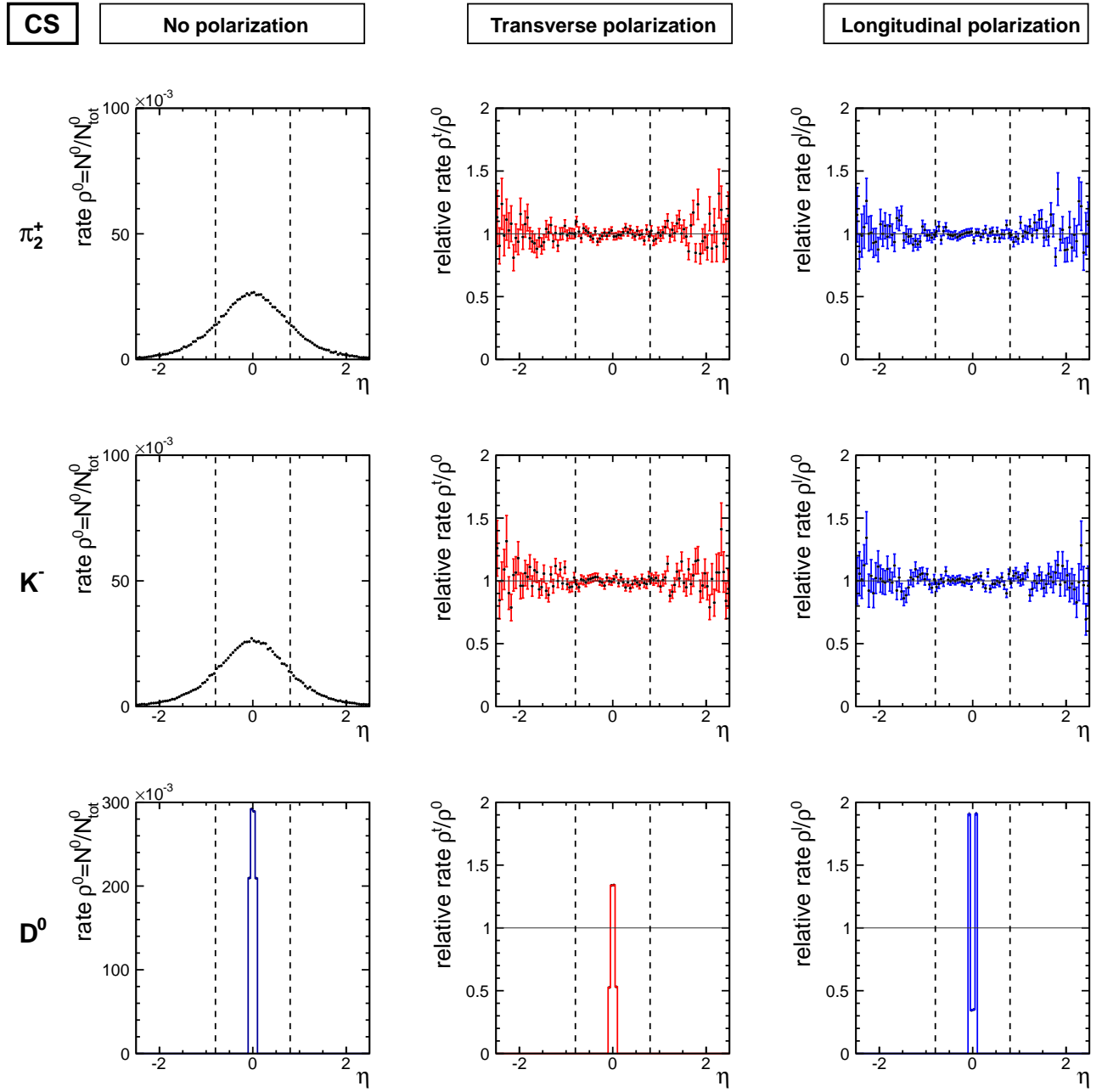


Figure A.2: Spatial distribution of D^0 and decay daughters K^- , π_2^+ from D^* -decay for different polarization states in the Collins-Soper frame with $|\vec{p}(D^*)| = 0.5 \text{ GeV}$, $\vec{p}(D^*) \parallel \vec{e}_x$ for 10^5 events.

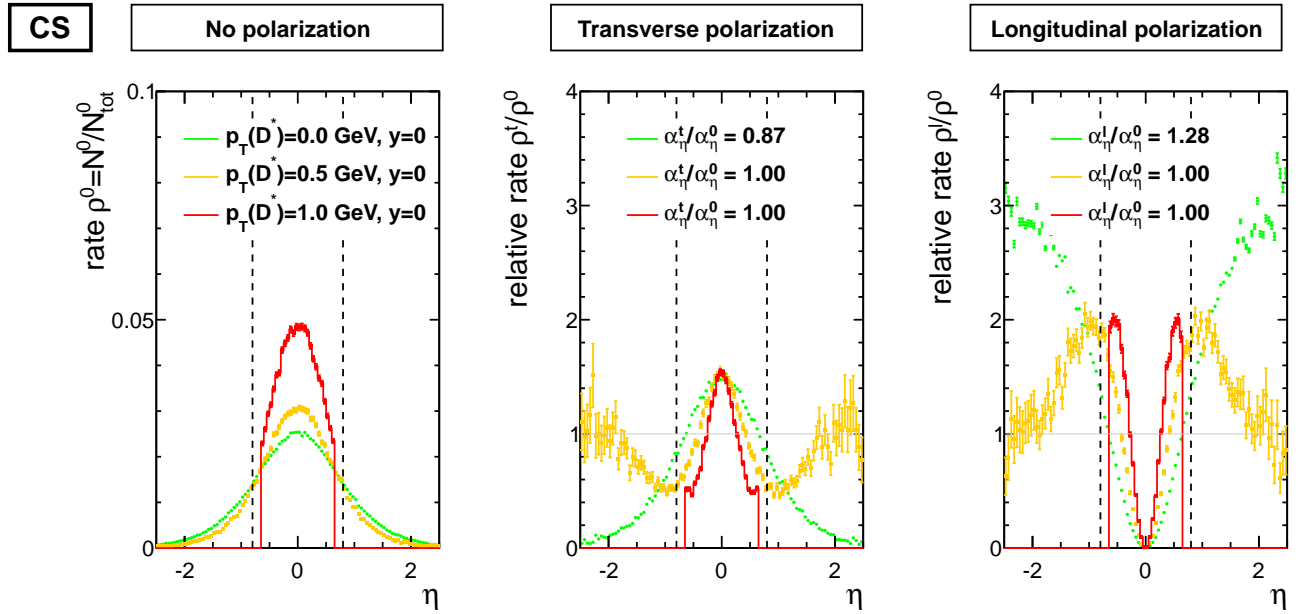


Figure A.3: Spatial distribution of π^+ from D^* -decay for different polarization states and rising momentum in the Collins-Soper frame. $|\vec{p}(D^*)| \in \{0.0, 0.5, 1.0\} \text{ GeV}$, $\vec{p}(D^*) \parallel \vec{e}_x \cdot 10^6$ events for $p_x = 0.5, 1.0 \text{ GeV}$, 10^7 events for $p_x = 0.0 \text{ GeV}$.

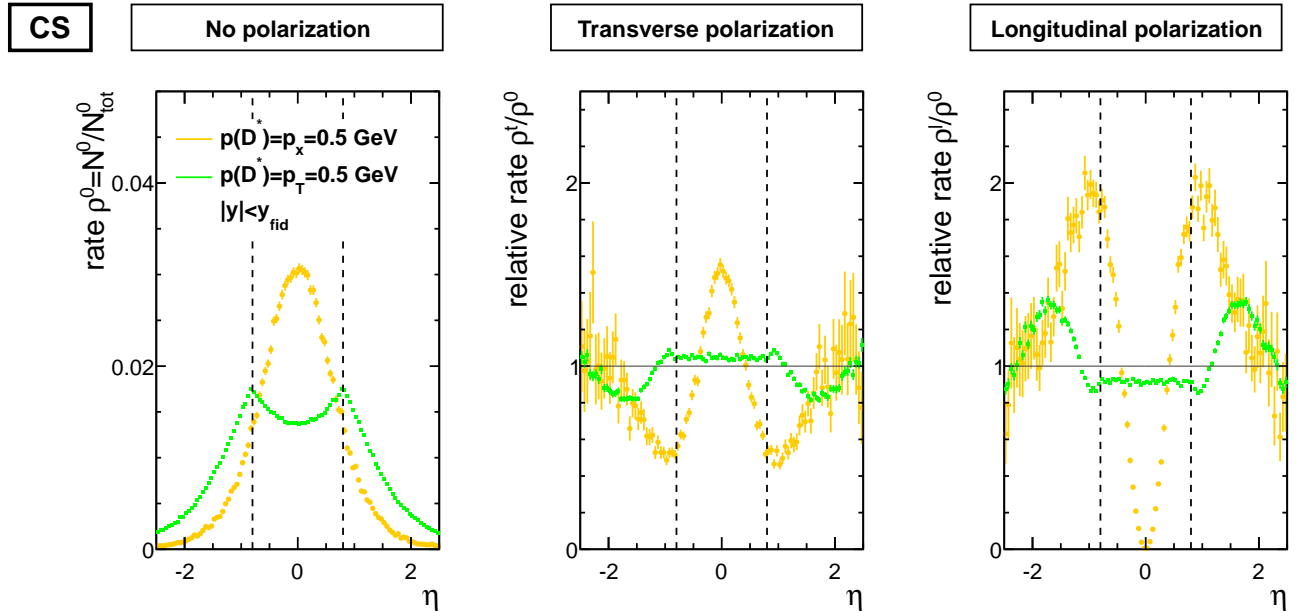


Figure A.4: Spatial distribution of soft pion from D^* -decay for different polarization states in the Collins-Soper frame with $p_T(D^*) = 1 \text{ GeV}$. Comparison of $y(D^*) = 0$, $y(D^*) \in [-0.5, +0.5]$ for 10^6 events.

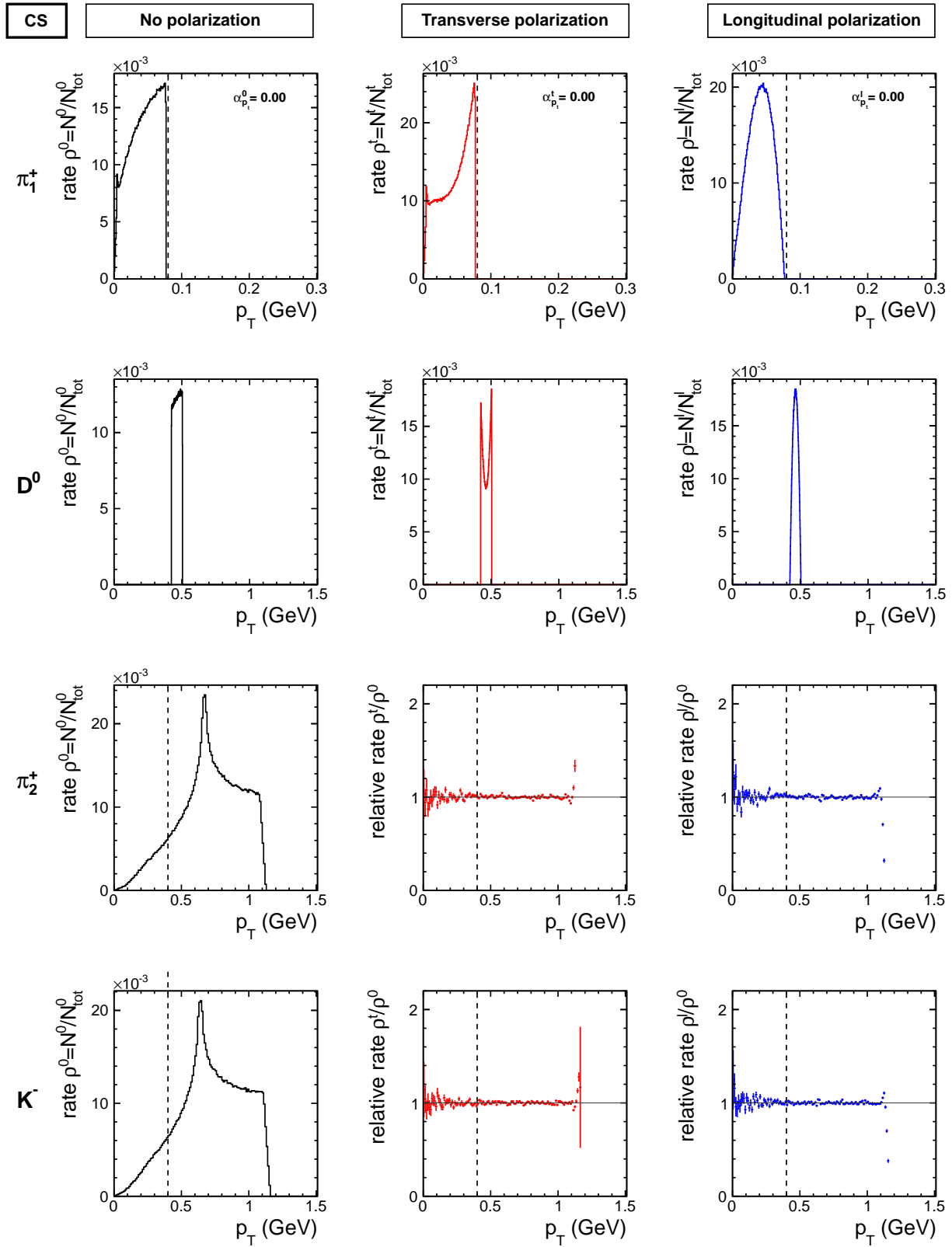


Figure A.5: p_T -spectra of D^* decay products (soft pion π_1^+ , D^0 from primary decay and K^- , π_2^+ from secondary decay) in lab frame with polarization in the helicity frame and $p_T(D^*) = 0.5$ GeV, $y(D^*) \in [-0.5, +0.5]$ for 10^6 events.

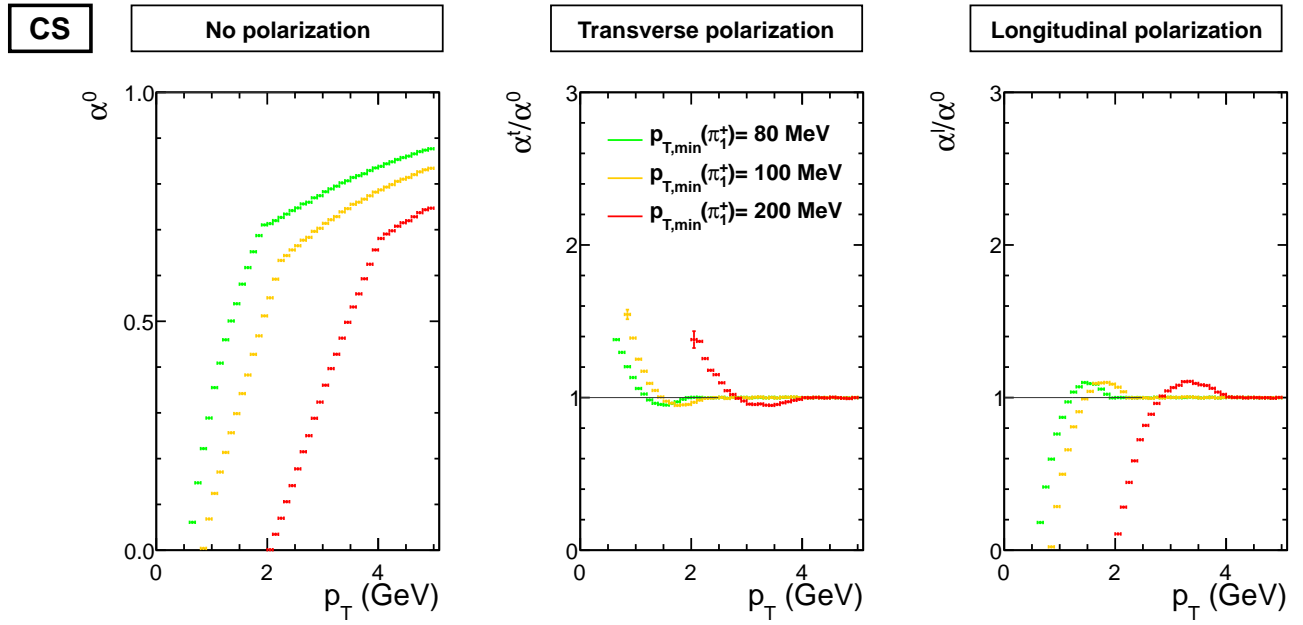


Figure A.6: Acceptance effect due to p_t -cut in the Collins-Soper frame for different sets of p_T -cuts. The corresponding p_T -cuts for the secondary decay particles are listed in table 3.3. $p_T(D^*) \in [0, 5] \text{ GeV}$, 10^6 events per p_T -bin

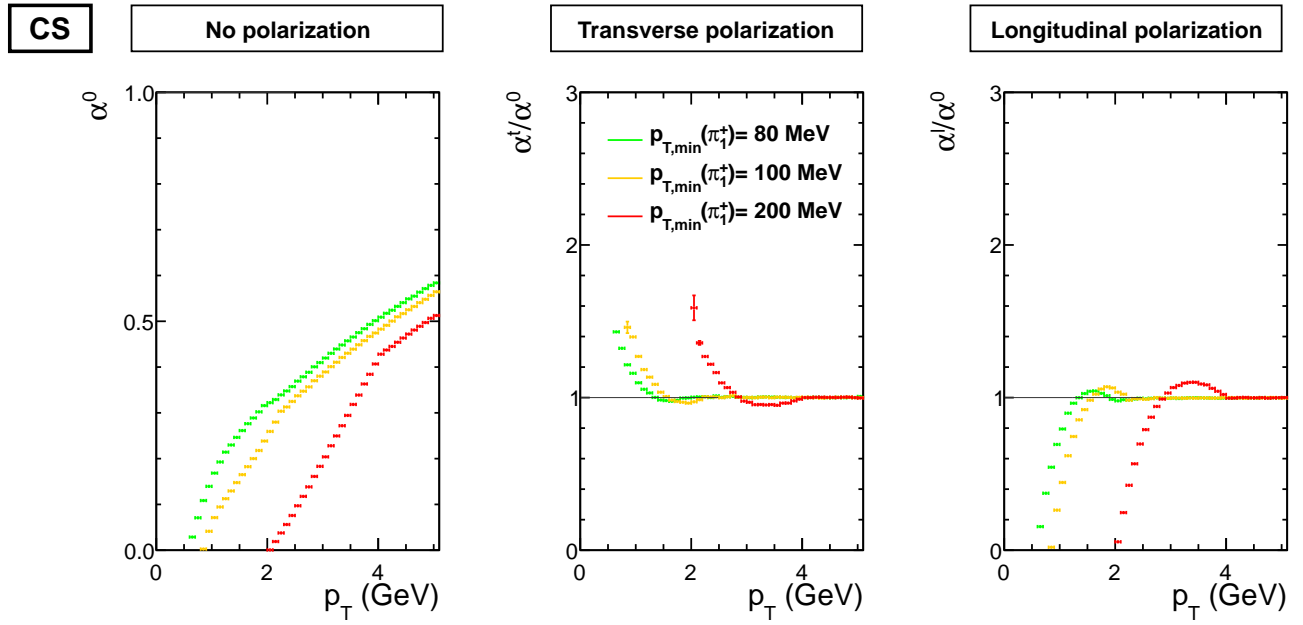


Figure A.7: Acceptance α of D^* meson for different sets of p_T -cuts 3.3 in the Collins-Soper frame for different polarization states. $\Delta p_T = 0.1$ GeV. $p_T(D^*) \in [0, 5]$ GeV for 10^6 events per p_T -bin.

B Tabulated values of relative acceptance for different p_T cuts

This section holds tabular representations of the calculated combined relative acceptancies $\alpha_{rel}^{t,l}$ for soft pion cuts $p_T \in \{80, 100, 200\}$ MeV. The values for each cut are shown for transverse and longitudinal polarization in helicity and Collins-Soper frame. All values were rounded to 2 decimals. Values above $\hat{p}(\alpha_{p_T})$ with $\alpha_{rel} \in [0.99, 1.01]$ are represented as 1.00 ± 0.01 . All relative acceptance values for transverse momentum above the illustrated p_T range are in $[0.99, 1.01]$, all values below the illustrated p_T range are 0.

Calculation of upper boundaries \hat{p}_T

The upper boundary \hat{p}_T of the acceptance effect is defined by the value at which for all $p_T \geq \hat{p}_T$, $\alpha_{rel}^{t,l}(p_T)$ is within $[0.99, 1.01]$ for both longitudinal and transversal polarization for a certain reference frame. As discussed in chapter 5.3.2, this boundary is mainly defined by the soft pion p_T cut. It should therefore be independent of the reference frame. Nevertheless, for soft pion cuts at 80 and 100 MeV, the η -cut leads to an additional relative effect of $\approx 1\%$ for D^* mesons with p_T just above $\hat{p}_T(\alpha_{p_T})$. This effect diminishes to $< 1\%$ within a few 100 MeV. It is only observed for the helicity frame due to the specific spatial distributions dependent on the D^* momentum axis. The upper boundary of the combined acceptance effect $\hat{p}_T(\alpha)$ is thus shifted to higher p_T compared to $\hat{p}_T(\alpha_{p_T})$ in these cases. This leads to different values of $\hat{p}_T(\alpha)$ for helicity and Collins-Soper frame listed in table 5.3. Due to the insignificance of these marginal effects on the cross section measurement, no further timely calculations with higher statistics were performed to reduce the fluctuations.

$p_T(D^*)$ (GeV)	Helicity frame		Collins-Soper frame	
	α_{rel}^t	α_{rel}^l	α_{rel}^t	α_{rel}^l
0.5	0	0	0	0
0.6	0	0	0	0
0.7	0.59	1.8	1.43	0.15
0.8	0.75	1.5	1.32	0.37
0.9	0.89	1.2	1.21	0.54
1	0.97	1.1	1.16	0.69
1.1	1.03	0.95	1.1	0.79
1.2	1.07	0.87	1.05	0.9
1.3	1.09	0.82	1.03	0.96
1.4	1.11	0.8	1	1
1.5	1.1	0.8	0.98	1
1.6	1.08	0.82	0.98	1
1.7	1.06	0.86	0.98	1
1.8	1.04	0.91	0.98	1
1.9	1.01	0.98	1	1
2	0.98	1	1.00 ± 0.01	0.99
2.1	0.99	1.00 ± 0.01	1.00 ± 0.01	0.98
2.2	1.00 ± 0.01	1.00 ± 0.01	1.00 ± 0.01	0.99
2.3	1.00 ± 0.01	1.00 ± 0.01	1.00 ± 0.01	0.98
2.4	1.00 ± 0.01	1.00 ± 0.01	1.00 ± 0.01	1.00 ± 0.01

Table B.1: Relative acceptance values for soft pion cut at $p_T = 80$ MeV for transverse and longitudinal polarization in helicity and Collins-Soper frame for $p_T(D^*) \in [0, 2.4]$ GeV with $\Delta p_T = 0.1$ GeV and 10^6 events per p_T bin.

$p_T(D^*)$ (GeV)	Helicity frame		Collins-Soper frame	
	α_{rel}^t	α_{rel}^l	α_{rel}^t	α_{rel}^l
0.7	0	0	0	0
0.8	0	0	0	0
0.9	0.35	2.3	1.5	0.019
1	0.58	1.9	1.4	0.26
1.1	0.72	1.5	1.3	0.44
1.2	0.86	1.3	1.2	0.62
1.3	0.94	1.1	1.1	0.74
1.4	1	0.98	1.1	0.85
1.5	1.1	0.89	1	0.92
1.6	1.1	0.83	1	0.98
1.7	1.1	0.8	0.98	1
1.8	1.1	0.79	0.97	1.1
1.9	1.1	0.81	0.97	1.1
2	1.1	0.85	0.96	1.1
2.1	1.1	0.88	0.97	1
2.2	1	0.94	0.99	1
2.3	1.00 ± 0.01	1.00 ± 0.01	1.00 ± 0.01	0.98
2.4	1.00 ± 0.01	1.00 ± 0.01	1.00 ± 0.01	1.00 ± 0.01

Table B.2: Relative acceptance values for soft pion cut at $p_T = 100$ MeV for transverse and longitudinal polarization in helicity and Collins-Soper frame for $p_T(D^*) \in [0, 2.4]$ GeV with $\Delta p_T = 0.1$ GeV and 10^6 events per p_T bin.

$p_T(D^*)$ (GeV)	Helicity frame		Collins-Soper frame	
	α_{rel}^t	α_{rel}^l	α_{rel}^t	α_{rel}^l
1.9	0	0	0	0
2	0	0	0	0
2.1	0.13	2.7	1.6	0.055
2.2	0.31	2.4	1.4	0.25
2.3	0.5	2	1.3	0.43
2.4	0.62	1.8	1.2	0.57
	0.75	1.5	1.2	0.7
2.5	0.84	1.3	1.1	0.79
2.6	0.93	1.2	1.1	0.87
2.7	0.98	1	1	0.94
2.8	1	0.94	1	0.99
2.9	1.1	0.87	0.98	1
3	1.1	0.81	0.97	1.1
3.1	1.1	0.78	0.95	1.1
3.2	1.1	0.76	0.95	1.1
3.3	1.1	0.76	0.95	1.1
3.4	1.1	0.78	0.95	1.1
3.5	1.1	0.79	0.95	1.1
3.6	1.1	0.82	0.96	1.1
3.7	1.1	0.86	0.96	1.1
3.8	1	0.9	0.98	1
3.9	1	0.95	0.99	1
4	1	1	1	1
4.1	1.00 ± 0.01	1.00 ± 0.01	1.00 ± 0.01	1.00 ± 0.01

Table B.3: Relative acceptance values for soft pion cut at $p_T = 100$ MeV for transverse and longitudinal polarization in helicity and Collins-Soper frame for $p_T(D^*) \in [0, 2.4]$ GeV with $\Delta p_T = 0.1$ GeV and 10^6 events per p_T bin.

C Influence of p_T -cuts on secondary pions and kaons

The p_T cuts listed in table 3.3 were applied for the performed simulations. In the phase of proof-reading, Robert Grajcarek [20], involved in the D^* cross section analyses at ALICE, remarked that the cuts applied to the secondary decay daughters π_2^+ and K^- are raised above the values shown in table 3.3 for higher D^* transverse momenta for the final analysis. As these values were not shown in the publications [7, 11], the tabulated values were applied for all D^* simulations. This leads to different *absolute* acceptance values for different p_T in figures 5.14, 5.15, 5.16, A.6, 5.17 and A.7 than in the specific analysis. As discussed in section 5.3.1, it will however have no influence on the *relative* acceptance between the different polarization states. Thus, the final results on cross sections will not be influenced by choosing the fixed cuts.

Acknowledgments

I would like to thank Prof. Dr. Johanna Stachel for giving me the opportunity to carry out my bachelor thesis in her group.

Special thanks go to my supervisor Dr. Kai Schweda for his support and motivating talks. I derived great benefit from the discussions and his explanation of various principles of high energy particle physics and nuclear physics. I am grateful to have had the opportunity to visit CERN and get an insight into the context of my work within a large collaboration of international physicists.

I greatly appreciated the help of Robert Grajcarek with the technical issues of `AliRoot` and with all questions concerning the D^* cross section analyses.

I owe special thanks to Michael Winn, Manuel Meske, Jannes Jegminat and Nora El Mamoun for proof-reading my thesis. I would also like to express my thanks to the Heidelberg members of the ALICE collaboration for their help with different issues as well as their feedback: Jochen Klein, Johannes Stiller, Daniel Lohner, Felix Reidt, Felix Mücke, Stephan Stiefelmaier and many more.

I wish to express my gratitude to my parents for their support of my studies.

This work has been supported by the Federal Ministry of Education and Research under promotional reference 06HD197D and by HA216/EMMI.

Erklärung

Ich versichere, dass ich diese Arbeit selbstständig verfasst und keine anderen als die angegebenen Quellen und Hilfsmittel benutzt habe.

Heidelberg, _____

Felix Benjamin Schäfer